Theses and Dissertations | 1. Thesis and Dissertation Collection, all items

---

1972-03

Jet penetration and interaction at a sonic throat.

Frick, Kenneth Edwin.

Monterey, California. Naval Postgraduate School

---

http://hdl.handle.net/10945/16227

JET PENETRATION AND INTERACTION
AT A SONIC THROAT

Kenneth Edwin Frick

NAVAL POSTGRADUATE SCHOOL
Monterey, California
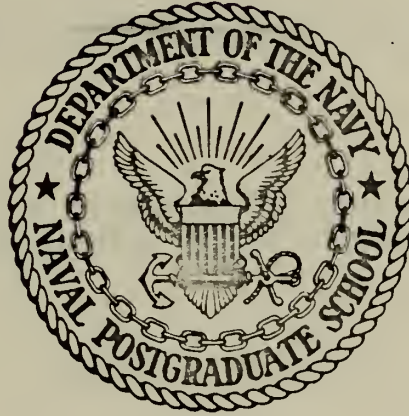
THESIS

Jet Penetration and Interaction at a Sonic Throat

by

Kenneth Edwin Frick

Thesis Advisor   R. H. Nunn

March 1972

Jet Penetration and Interaction at a Sonic Throat

by

Kenneth Edwin Frick
Lieutenant, United States Navy
B.S.W.E., Ohio State University, 1966

Submitted in partial fulfillment of the
requirements for the degree of

MECHANICAL ENGINEER

from the

NAVAL POSTGRADUATE SCHOOL
March 1972

ABSTRACT

This thesis describes the results of an investigation of the throttling effects of a transverse jet when injected into a sonic throat. The process, commonly referred to as aerodynamic throttling, was studied both analytically and experimentally.

An analytical model is developed utilizing momentum considerations. This model successfully predicts the measured throttling results for 90° injection and mainstream flow reductions up to approximately 60 percent. The agreement between theory and experiment becomes less satisfactory as the upstream angle of injection is increased and at extremely high throttling conditions.

An experimental program is described in which a two-dimensional nitrogen jet is injected into the mainstream through slots of various widths and inclinations. Visual flow patterns are shown to qualitatively describe the nature of the interaction between the jet and the mainstream.

TABLE OF CONTENTS

3

LIST OF TABLES

LIST OF ILLUSTRATIONS

NOMENCLATURE

a	Speed of Sound
B	Mainstream duct height
C_D	Discharge coefficient
d_t	Width of jet nozzle throat
F_x	Effective pressure force on "windward" side of jet; acting in the x-direction
h	Maximum height of sonic line above the wall
H	Jet slot width nondimensionalized by the mainstream duct height d_t/B
$\dot{m}$	Mass Flow Rate
M	Mach number
P	Pressure
T	Temperature
V_e	Exit velocity of jet
x,y	Coordinates along, or normal to wall, respectively
α	Angle of jet injection with respect to the vertical
γ	Ratio of specific heats
ρ	Density

SUBSCRIPTS

j	Jet conditions
m	Mainstream conditions
r	Reference conditions based on mainstream flow with no jet injection
0	Upstream conditions for mainstream
1	Mainstream conditions at point of injection
2	Mainstream conditions at point of maximum jet penetration

o   Stagnation conditions

*   Sonic conditions

FUNCTION DEFINITIONS

A(M)   Area ratio in locally isentropic flow

$$= \frac{1}{M} \left[\frac{1 + \frac{\gamma-1}{2} M^2}{\frac{\gamma+1}{2}} \right]^{\frac{\gamma+1}{2(\gamma-1)}}$$

P(M)   Pressure ratio in locally isentropic flow

$$= \left[1 + \frac{\gamma-1}{2} M^2 \right]^{\frac{\gamma}{1-\gamma}}$$

ACKNOWLEDGMENTS

I. INTRODUCTION

Seventeen years ago an article was published by Manoury, et.al.
[Ref. 1] proposing an exit plane aerodynamic nozzle for a jet engine.
This article pioneered the general concept of aerodynamic throttling.
Aerodynamic throttling is the process by which the mass flow rate of a
primary flow is controlled (throttled) by injecting a secondary (jet)
flow into the mainstream. The jet/mainstream interaction creates what
is referred to as an "aerodynamic throat" and has the effect of reducing
the mainstream mass flow rate. Since Manoury's article in 1955, the
feasibility of aerodynamic throttling has been shown experimentally
[Ref. 2-4] and predicted analytically [Ref. 5-7]. The knowledge gained
from these studies has been used by designers of systems that involve
the injection of one fluid into another such as variable-throat nozzles,
combustion chambers, and rocket nozzles cooled by injection.

This investigation was undertaken with the idea of applying the
principle of aerodynamic throttling to a fluidic device which could be
used in a missle control system. It was envisioned that a modified pro-
portional amplifier, with throttling control, could be used as a moment
producer for a missile steering system employing external jets. The
advantage of such a device would lie in the fact that during the no-
control phase of operation, the gas expended by the fluidic control
system could be throttled thereby saving gas and allowing for either
more control time, or a reduction in required control gas with a
resulting increase in missile payload.

An important aspect of the aerodynamic throttling process is the
extent to which the jet to mainstream total pressure ratio affects the

penetration of the jet into the mainstream. This study attempts to improve the analytical prediction of the penetration height of the jet and also to extend the information available about the throttling process by experimentally determining the effect of high total pressure ratios. Previous investigators have not gone above jet to mainstream total pressure ratios of 5:1.

II. ANALYSIS

A. GENERAL CONSIDERATIONS

The goal of this study is to examine the jet penetration and throttl-
ing characteristics of a transverse jet injected into a sonic throat.
The jet, shown in Fig. 1, is sonic, underexpended, two-dimensional and
inclined at an angle α into the mainstream.
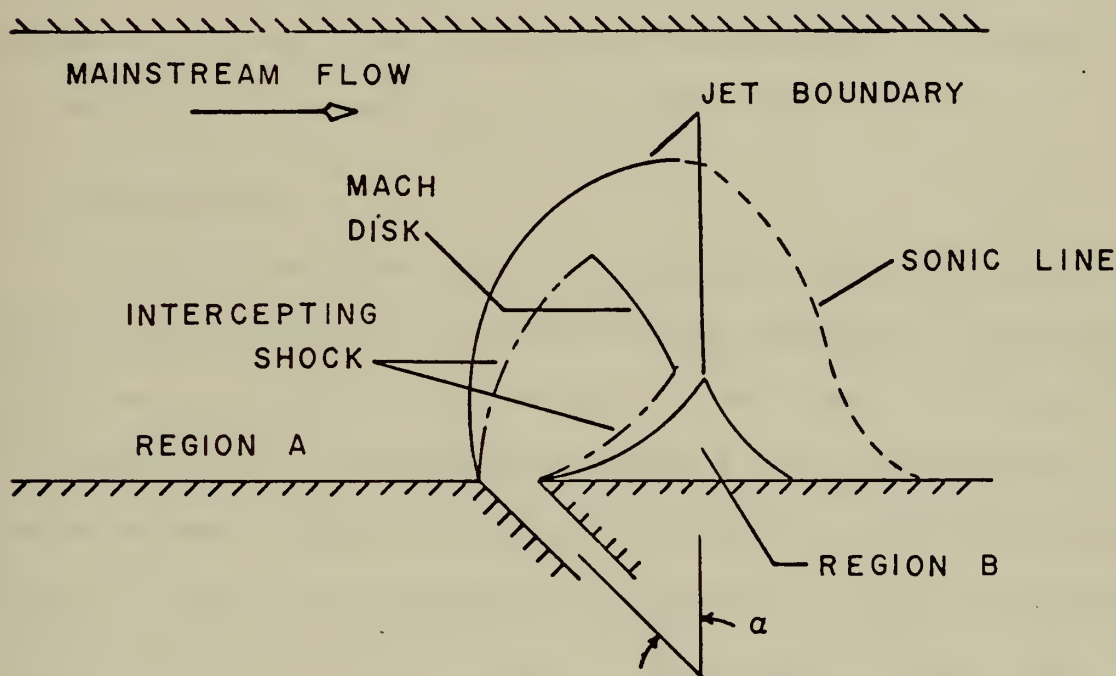

Figure 1. Region of Interest.

The basic structure of the jet in the vicinity of the nozzle exit is
similar to that of a free jet expanding into a quiescent atmosphere
except that the pressure in region A (windward side) is higher than that
in region B (bubble side). This pressure imbalance results in a jet
plume that is skewed relative to the nozzle axis. For a given injector

geometry and specific gas properties, the jet total pressure and the exterior pressure in regions A and B determine the location of the jet boundaries. The jet flow in the core of the plume quickly becomes over-expanded and must pass through a strong jet shock while the flow along the boundary of the jet passes through a series of oblique shocks and remains supersonic. The strong jet shock, known as the Mach disk, is nearly normal to the jet flow direction. The jet flow immediately down-stream of the Mach disk is subsonic and at a pressure that is higher than the mainstream pressure. Beyond this point the jet reaccelerates and expands in an attempt to achieve pressure equilibrium with the mainstream. Mixing between the jet and the mainstream is considered to be negligible in the region prior to the Mach disk.

B. JET PENETRATION

In the jet penetration studies conducted by Schetz and Billig [ref 8] and Orth and Funk [Ref. 9] the characteristic dimension of the inter-action region was taken to be the height to the center of the Mach disk. This dimension was considered to be a measure of the jet penetration into the mainstream. Barnes, et.al. [Ref. 10] as well as Spaid and Zukoski [Ref. 11] chose as the characteristic dimension the height of the sonic line occurring in the jet at a short distance beyond the Mach disk. The actual penetration of the jet can only be defined in terms of its effect upon the crossing flow. The characteristic height, whether that of the Mach disk or the sonic line, is useful mainly as a scale for the pene-tration. Both of these heights have been found to be valid parameters for the correlation of jet interaction data. In this analysis the sonic line is used as a more convenient characteristic height and, in addition, it is felt that this measure is more nearly the actual or "effective"

12

depth of penetration as discussed below. To the extent that the calcula-
ted penetration is the actual penetration, the throttling characteristics
of the system can be calculated by a direct application of the principle
of mass flow continuity.

As the jet is turned by the bounded mainstream, the Mach disk becomes
more nearly perpendicular to the wall. In this configuration, a measure
of jet penetration based on the distance to the center of the Mach disk
would only account for the penetration of a portion of the jet. Simply
adding half the width of the Mach disk to this height would still not
account for the full penetration. Vick, et.al. [Ref. 12] has shown that
for three-dimensional free jets at low total pressure ratios, the Mach
disk occurs close to the point at which the jet plume achieves its
maximum width and that the Mach disk diameter is no more than sixty
percent of the maximum jet diameter. It appears reasonable then to
assume that for a two-dimensional jet the maximum penetration into a
bounded mainstream would be some distance greater than the height to
the center of the Mach disk.

Although the flow immediately behind the Mach disk is subsonic and
the mainstream would be expected to stronly affect the flow in this
region, there is jet flow along the windward boundary of the jet that
has not passed through the Mach disk and remains supersonic for some
distance downstream of the Mach disk. Vaughan [Ref. 13] and Maurer
[Ref. 14] have observed, using shadowgraphs and oil films respectively,
that the jet achieves a sonic velocity within a very short distance after
the Mach disk and that negligible mixing occurs between the jet and
mainstream prior to the sonic line. Thus, it is hypothesized that the
supersonic flow along the boundary shields the subsonic core of the jet

13

from massive mixing with the mainstream until the region of the sonic line is reached. Beyond this point it is assumed that the jet loses its identity, mixes with the mainstream, and ceases to affect the mainstream in the sense of penetration or throttling.

C. METHODS OF ANALYSIS

1. Previous Work

The problem of a secondary jet issuing into a bounded mainstream for the purpose of throttling the primary flow has been analyzed by numerous investigators in the past. In a recent analysis, Nunn [Ref. 15] makes use of a momentum balance across a control volume which includes both the mainstream and the jet. This momentum balance is then combined with continuity expressions for the mainstream and the jet along with a statement of pressure equilibrium between the jet and mainstream at the point of maximum penetration. To account for jet total pressure losses, it is noted that the strongest shock that can occur in the jet is at a jet Mach number which corresponds to an isentropic jet expansion to the critical mainstream static pressure. The solution of the system of equations presented in Nunn's work is based on the assumption that the strongest shock (i.e., the Mach disk) does occur in the jet and that it is located at the point of maximum penetration. It is felt that this assumption places an unrealistic constraint upon the flow field when a wide range of total pressure ratios is considered.

Nunn's analysis determines the shock strength purely on the basis of the ratio of total pressures:

$$\frac{P^o_j}{P^o_{mo}} \ .$$

14
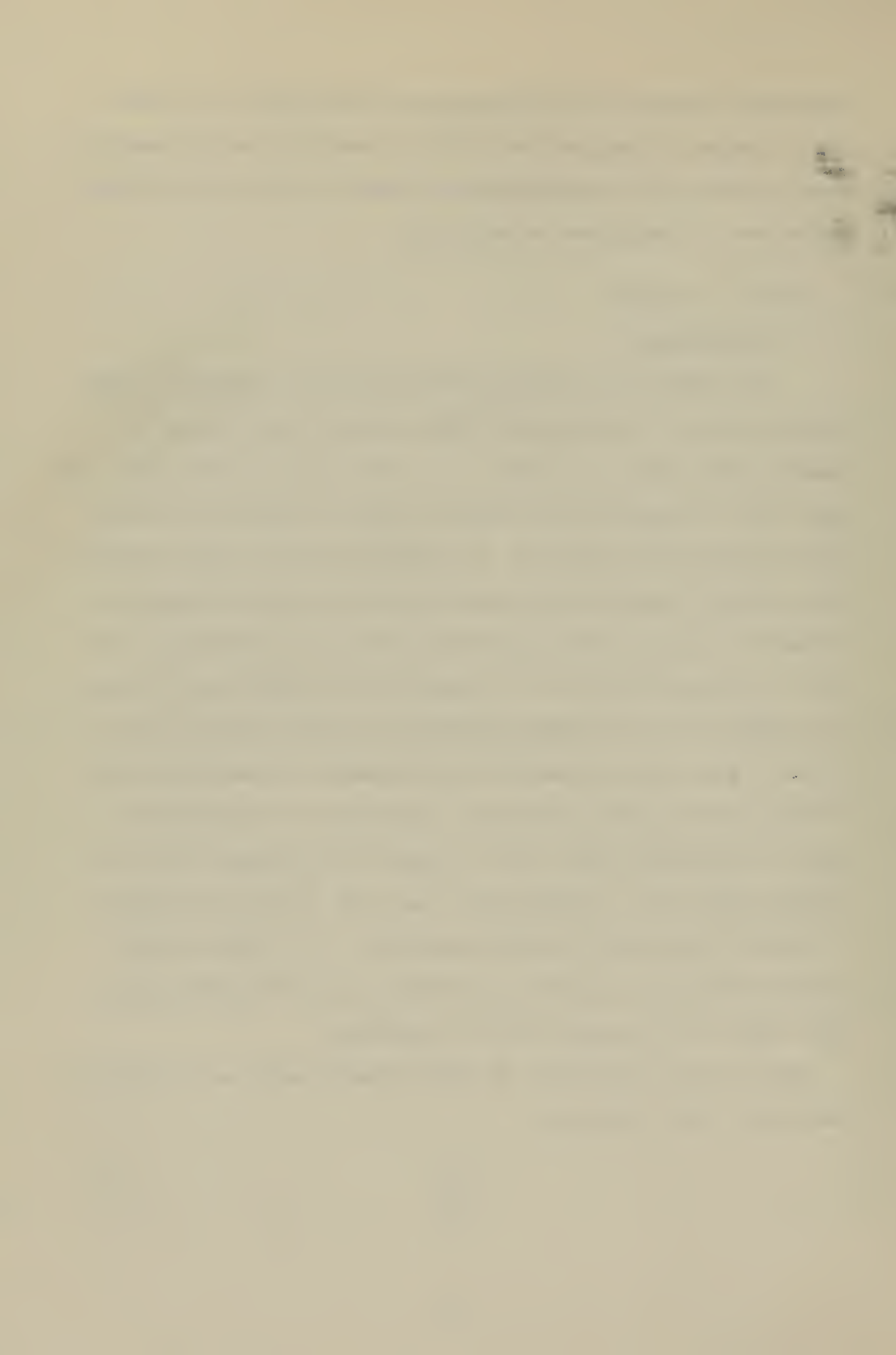
This is equivalent to assuming that the jet is exhausting into a quiescent atmosphere ($P_{mo}^O = P_\infty$), and does not take into consideration the crossing flow and the effect of the turning of the jet. Due to the curvature of the jet plume, the flow within the jet experiences an additional compression that will cause the shock to occur at a lower Mach number than would be predicted for a free jet.

It has been shown by Adamson and Nicholls [Ref. 16] as well as Vick, et.al. [Ref. 12] that for free jets, the distance to the Mach disk follows an approximately linear variation with:

$$\frac{P_j^O}{P_\infty}$$

when plotted on log coordinates. Additionally, Vick has shown that the ambient pressure (P_∞) has a definite effect on the Mach disk location. For a given pressure ratio:

$$\frac{P_j^O}{P_\infty}$$

the lower the ambient pressure, the less the distance from the nozzle exit to the Mach disk. Based on the above findings, it would seem unrealistic to assume that the Mach disk, for all pressure ratios:

$$\frac{P_j^O}{P_{mo}^O} \quad ,$$

would position itself at the point of maximum penetration.

It is advantageous to seek an analytical model whereby the jet boundaries as well as the Mach disk are more accurately predicted for jets which experience not only a different pressure on each side, but also encounter a varying pressure on the windward face. A computer program was written employing the method of characteristics to determine the

shape of the jet plume along with the Mach number distribution on the centerline. This program was successfully completed for jets which experience a constant pressure on each face, but attempts to modify the program to account for a varying pressure were discontinued for two main reasons. First, it is not known *a priori* just what the pressure distributions are on the faces of the jet, and secondly the complexity of the computer program that would be necessary to handle this problem by means of the method of characteristics was deemed to be prohibitive. Therefore, it was decided that an alternate approach to the problem was needed. For purposes of completeness, however, a brief description of the method of characteristics calculations, together with a computer listing, is included as Appendix A to this report. A primary consideration of this alternate approach was to avoid the assumption that the Mach disk occurs at any particular location in the jet.

2. Present Analysis

As indicated previously, the jet is assumed to be sonic at injection, underexpanded, two-dimensional and inclined at an angle α into the mainstream. The jet undergoes an initial isentropic expansion and is then recompressed by a strong normal shock, the Mach disk. The jet fluid leaving the Mach disk again expands to sonic velocities a short distance downstream. The flow is assumed to reattach itself to the wall and continue to flow parallel to it.

The dotted line in Fig. 2 is designated as the sonic line and is the transition from sonic to supersonic velocities. The actual geometry of the sonic line is unknown. The geometry has, however, no effect on the results of the analysis if it is assumed that the turning of the jet occurs prior to the sonic line so that the average momentum of the jet fluid at the sonic line is parallel to the wall. This

16

assumption is the same as that made by Barnes, et.al. [Ref. 10] and Cassel, et.al. [Ref. 17] in their studies of jets in an unbounded mainstream.
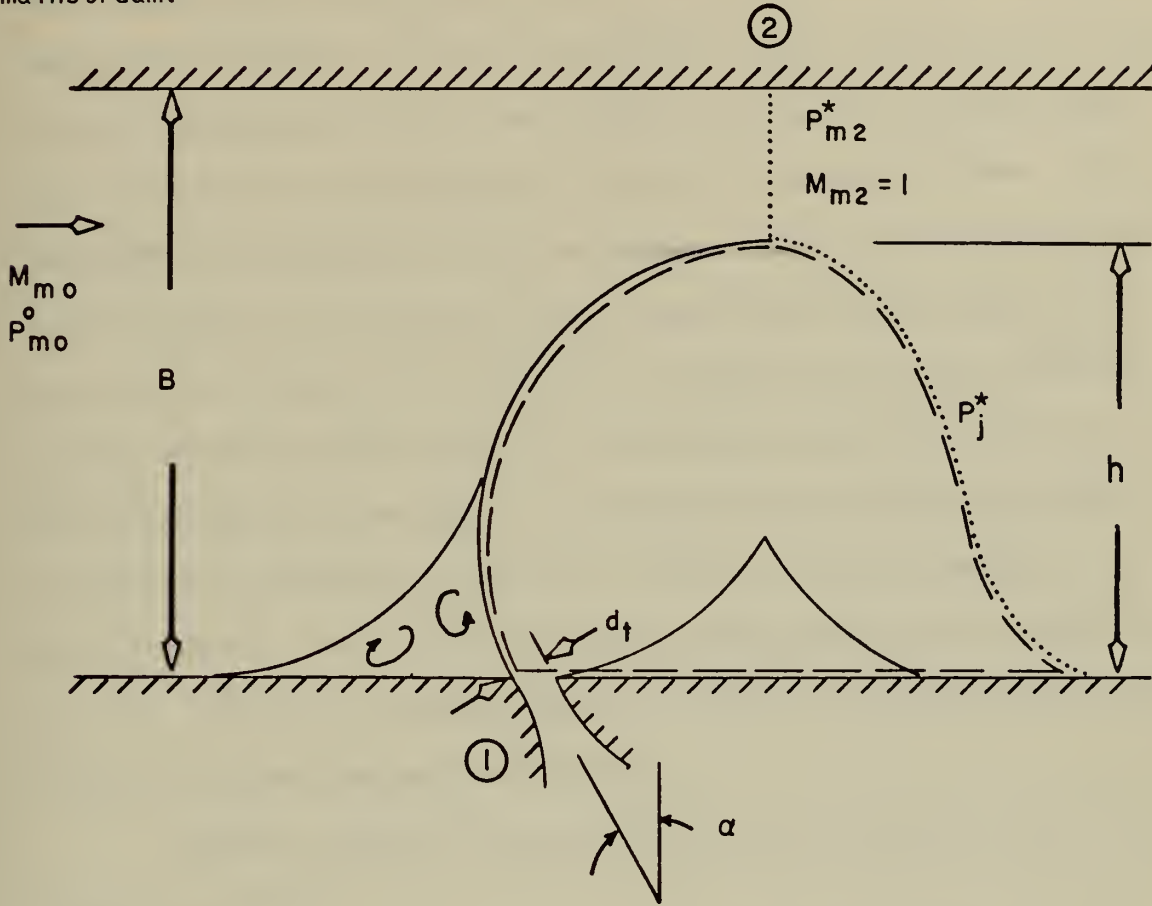
Figure 2.   Schematic Diagram of Throttling Region Showing Control Volume.

A control volume (dashed line in Fig. 2) is defined which is bounded by the windward face of the jet plume from the nozzle to the jet sonic line (this is also the point of minimum mainstream flow area), the jet sonic line to the wall, and the plane of the wall.

Conservation of jet momentum requires that the change in the x-component of momentum be equal to the forces in the x-direction acting upon the control volume. Recalling that the momentum vector of the jet fluid at the sonic line is assumed to be parallel to the wall, the conservation of momentum can be expressed as follows:

17

$$F_x - P_j^* \, h = \dot{m}_j \, [a^* + V_e \sin \alpha] \tag{1}$$

In this expression F_x is the average pressure force acting in the x-direction on the windward face of the jet and will be evaluated in subsequent paragraphs. It has been further assumed here that the shear stresses acting along the jet/mainstream interface do not contribute significantly to the x-component of the net force on the plume. This assumption is characteristic of earlier jet interaction analyses (including those previously mentioned) and is based upon the hypothesis that the drag due to shear will only play a significant role at downstream regions where turbulent mixing is the dominant exchange mechanism for mainstream and jet momentum. This assumption presupposes an initial transverse jet momentum sufficient to lead to a large penetration in a short distance. As the distance to jet maximum penetration increases (as, for instance the upstream angle of injection increases) the neglect of shear stresses becomes less credible.

Equating the mass flow rate at the nozzle throat to that at the sonic line yields:

$$\dot{m}_j = \rho_t \, d_t \, a_t = \rho^* \, h \, a^* = \gamma \left(\frac{2}{\gamma+1}\right)^{\frac{\gamma}{\gamma-1}} \frac{P_j^0 \, d_t}{a_t} \tag{2}$$

where the subscript (t) refers to conditions at the injection sonic throat. The latter relationship in Equation (2) restricts the analysis to conditions in which the jet behaves as an ideal gas and the process is adiabatic. Thus, for situations in which the jet total temperature varies widely from that of the mainstream, it may become necessary to consider the transfer of heat across the jet mainstream boundary. For the adiabatic process, $a^* = a_t$ and Equation (2) produces the following relationships:

$$\frac{\rho^*}{\rho_t} = \frac{\dot{d}_t}{h} = \frac{P_j^*}{P_t} = \frac{P^{o*}}{P_j^o} \tag{3}$$

It should be noted that Equations (2) and (3) are the same as those obtained by Barnes, et.al. [Ref. 10] in their study of transverse jets interacting with an unbounded free stream. Substituting Equations (2) and (3) into the momentum equation yields an expression for the maximum height of the sonic line above the wall:

$$\frac{h}{d_t} = \frac{P_j^o}{\frac{F_x}{h}} \left(\frac{2}{\gamma+1}\right)^{\frac{\gamma}{\gamma-1}} \left[\gamma\left(1 + \frac{V_e}{a_t}\sin\alpha\right) + 1\right]. \tag{4}$$

Since the experiments that were conducted for this study treated only jets which were sonic at injection, $V_e = a_t$, Equation (4) takes the final form of:

$$\frac{h}{d_t} = \frac{P_j^o}{\frac{F_x}{h}} \left(\frac{2}{\gamma+1}\right)^{\frac{\gamma}{\gamma-1}} \left[\gamma\left(1 + \sin\alpha\right) + 1\right]. \tag{5}$$

The height of the sonic line, h, as given by Equation (5), is a characteristic dimension of the flow field which according to the previous arguments is an estimate of the depth of jet penetration into the mainstream.

If Equation (5) could be solved directly for h, then it would be a simple matter to determine the effective throttling of the mainstream. The problem, however, lies in determining the effective average pressure, F_x/h, acting on the windward boundary. Since the mainstream is bounded on all sides, a sonic throat will be formed in the mainstream at the point of maximum jet penetration. The pressure acting on the windward

face of the jet is assumed to vary from the mainstream static pressure at station 1 [Ref. 15] down to P_m^* at station 2. See Fig. 2.

The effective average pressure acting on the windward boundary can be expressed in integral form as:

$$\frac{F_x}{h} = \frac{1}{h} \int_{y_1}^{y_2} P \, dy \tag{6}$$

Expressing this integral in terms of Mach number gives:

$$\frac{F_x}{h} = \frac{P_{mo}^o}{h} \int_{M_{mo}}^{1} P(M) \frac{dy}{dM} \, dM \tag{7}$$

Relating y to M

$$\frac{B-y}{B} = \frac{A}{A_1} = \frac{A(M)}{A(M_{mo})}$$

and differentiating y with respect to M gives:

$$\frac{dy}{dM} = - \frac{B}{A(M_{mo})} \frac{d}{dM} [A(M)] \tag{8}$$

Upon evaluating $\frac{d}{dM} [A(M)]$ Equation (8) becomes:

$$\frac{dy}{dM} = \frac{B \, A(M)}{A(M_{mo})} \left[\frac{1}{M} - \frac{\frac{\gamma+1}{2} M}{1 + \frac{\gamma-1}{2} M^2} \right]$$

and substitution of this expression into Equation (7) gives the following for the effective pressure:

$$\frac{F_x}{h} = \frac{B \, P_{mo}^o}{h} \int_{M_{mo}}^{1} P(M) \frac{A(M)}{A(M_{mo})} \left[\frac{1}{M} - \frac{\frac{\gamma+1}{2} M}{1 + \frac{\gamma-1}{2} M^2} \right] dM \; . \tag{9}$$

20

Finally, if Equation (9) is substituted into Equation (5) an equation in terms of the mainstream Mach number, M_{mo}, appears as follows:

$$M_{mo} \left[\frac{1 + \frac{\gamma-1}{2} M_{mo}^2}{\frac{\gamma+1}{2}} \right]^{\frac{\gamma+1}{2(1-\gamma)}} \int_{M_{mo}}^{1} \left(1 + \frac{\gamma-1}{2} M^2\right)^{\frac{\gamma+1}{2(\gamma-1)}} \left[\frac{1}{M^2} \left(\frac{2}{\gamma+1}\right) \left(1 + \frac{\gamma-1}{2} M^2\right) - 1 \right] dM$$

$$= \frac{d_t}{B} \frac{P_j^0}{P_{mo}^0} \left[\gamma (1 + \sin \alpha) + 1 \right] \left(\frac{2}{\gamma+1}\right)^{\frac{\gamma}{\gamma-1}} \tag{10}$$

For a given set of parameters $\frac{d_t}{B}$, α, and $\frac{P_j^0}{P_{mo}^0}$, Equation (10) can be solved for the mainstream Mach number M_{mo}.

From the isentropic area relationship:

$$\frac{A}{A^*} = \frac{B}{B - h} = A(M_{mo})$$

an expression for the maximum jet penetration, h, can be obtained:

$$\frac{h}{B} = \left[\frac{A(M_{mo}) - 1}{A(M_{mo})} \right] \tag{11}$$

D. THROTTLING CHARACTERISTICS

A reference mass flow rate is defined as that which would flow isentropically in the mainstream with no jet injection;

$$\dot{m}_r = K \, P_{mo}^0 \, B$$

where

$$K = \left(\frac{2}{\gamma+1}\right)^{\frac{\gamma+1}{2(\gamma-1)}} \left[\frac{\gamma}{RT_m^0} \right]^{\frac{1}{2}}$$
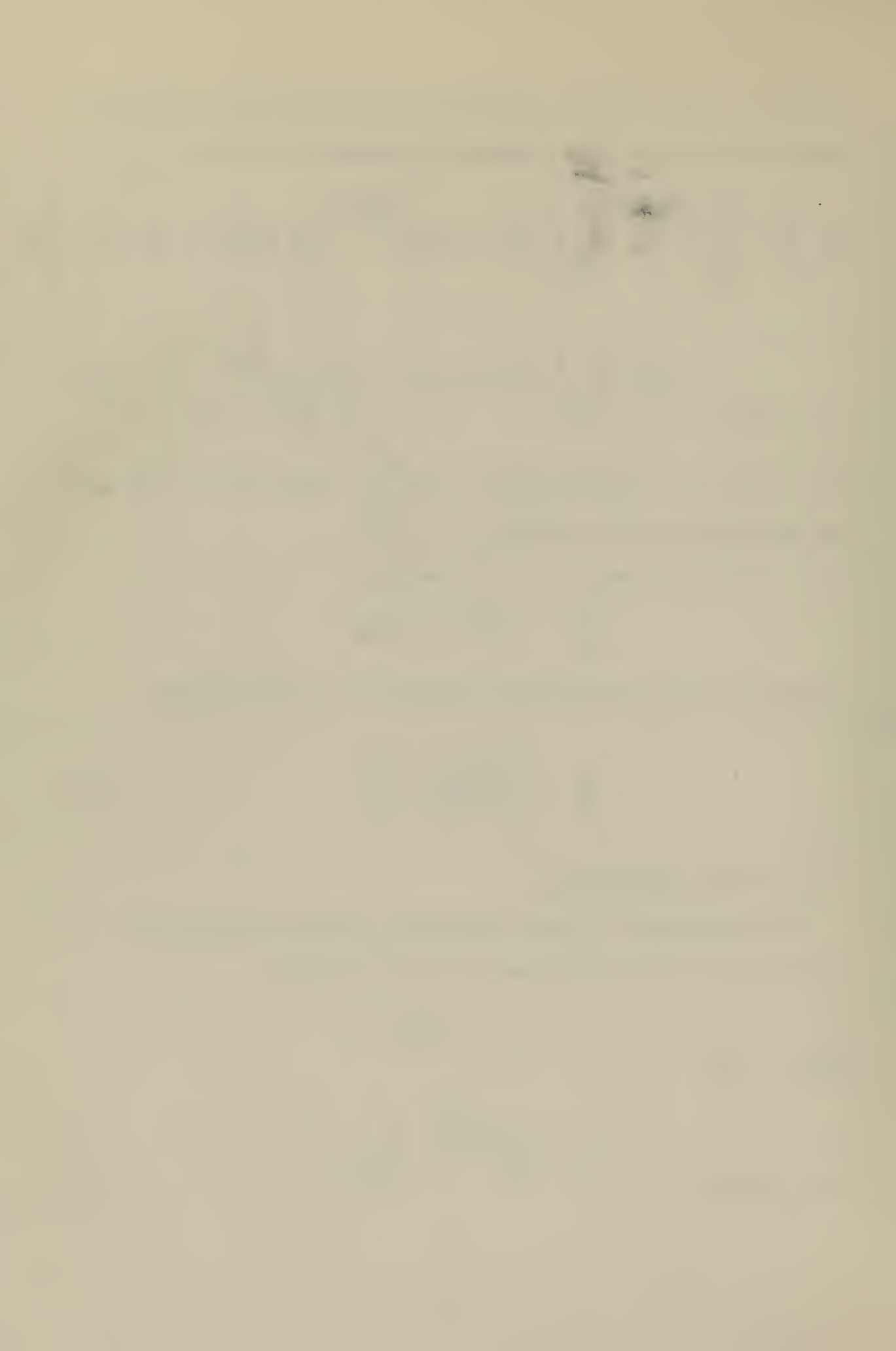
Using this reference mass flow rate, the throttled mainstream and jet mass flow rates may be expressed in nondimensional terms as:

$$\frac{\dot{m}_m}{\dot{m}_r} = \frac{1}{A(M_{mo})} \qquad (12)$$

$$\frac{\dot{m}_j}{\dot{m}_r} = \frac{d_t \; P^o_j}{B \; P^o_{mo}} \qquad (13)$$

The theoretical curves for flow throttling are shown in Figure 3.
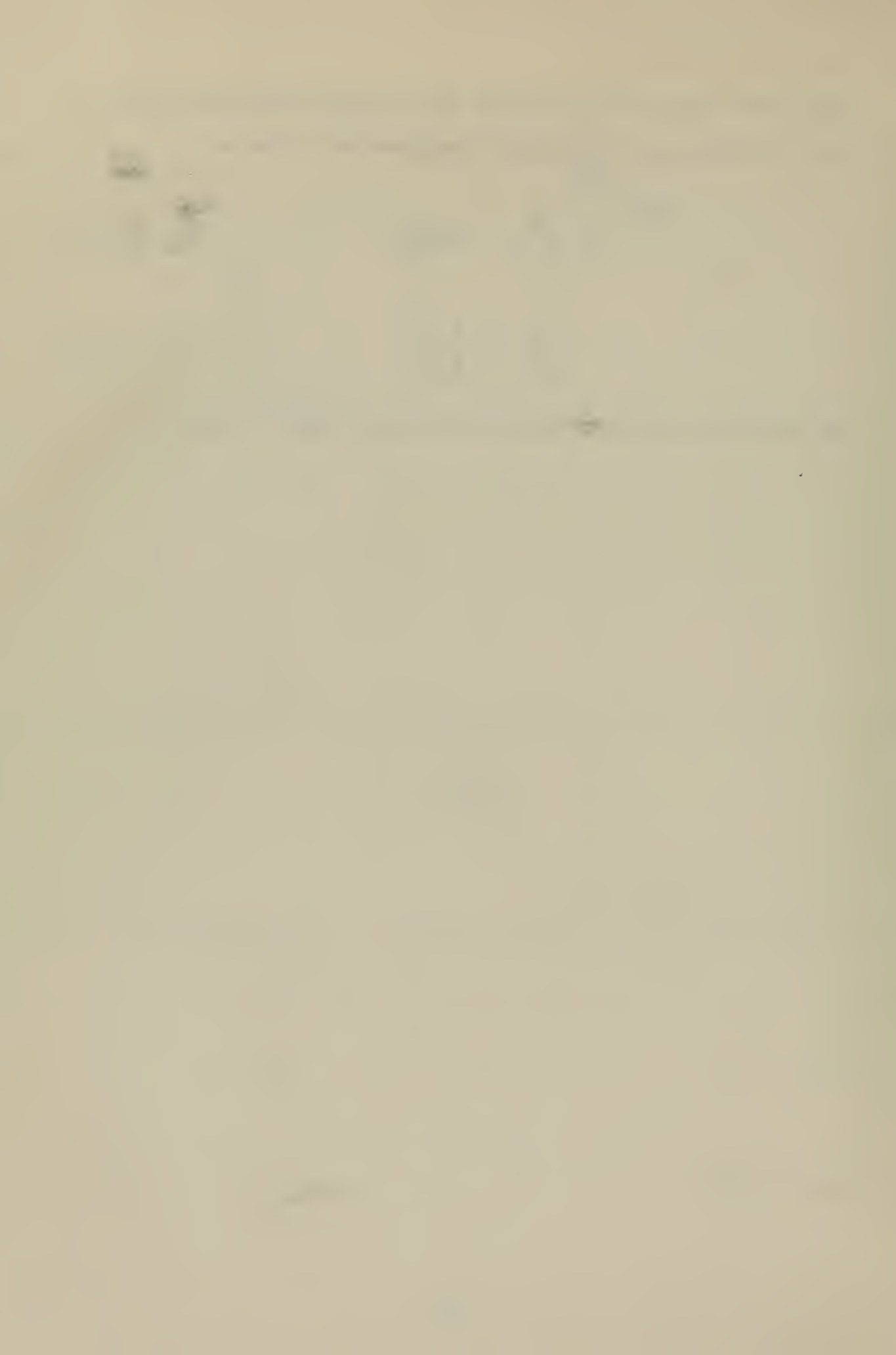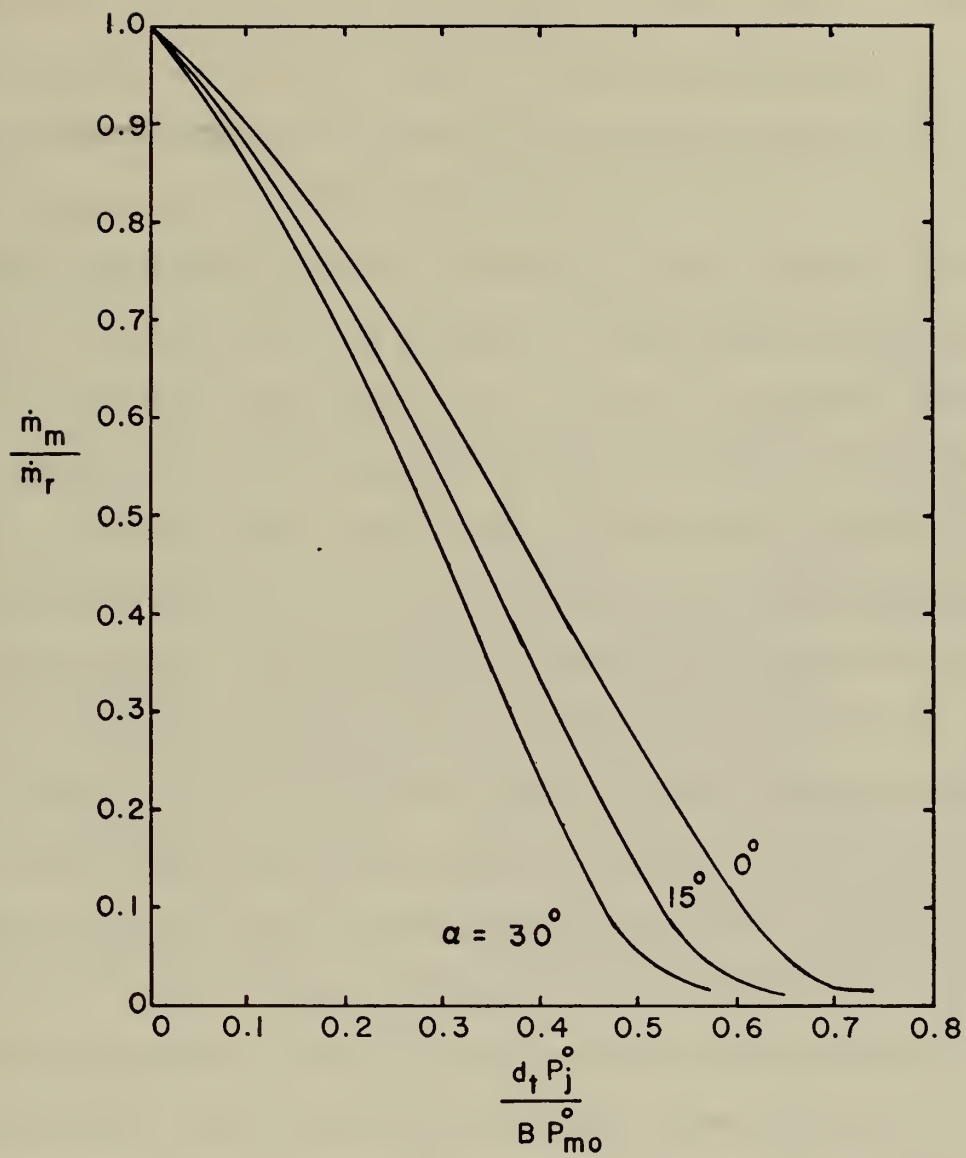
Figure 3. Throttling for Various Injection Angles (Unmodified Theory).

III. APPARATUS AND EXPERIMENTAL METHODS

The goals of the experimental portion of this study have been to evaluate the analytical model and examine the throttling effects of a transverse jet with various slot widths, d_t, and angles of injection, α, when injected into a sonic throat. To achieve these goals, it was desired to experimentally determine the mass flow rates of the mainstream and jet during the throttling process.

The experimental apparatus consisted of four distinct functional units: the first being the primary air flow system; the second being the test section itself; the third is the jet or secondary flow system; and, the fourth is the instrumentation for gathering flow information.

The primary system, shown in Fig. 4, consisted of a 200 psig air compressor and two 117 cu. ft. tanks. With both tanks pressurized to maximum capacity, it was possible to conduct blow-down tests of approximately one minute duration with a reference mass flow rate of 1.19 lbm/sec. The air left the tanks and passed through a pressure regulating valve just downstream of each tank. The pressure regulators were remotely controlled by a compressed nitrogen control system and were capable of regulating the mainstream pressure from 0 psig to 150 psig. After the regulators, the flow from both tanks was combined in a single 3-inch pipe in which was installed a remote controlled on-off valve. Downstream of the on-off valve, the 3-inch pipe was fitted with a standard ASME flat plate orifice which was used to obtain mass flow measurements for the primary system. The air then flowed into a 5-inch pipe and finally to a transition section that changed the circular cross-section to a rectangular cross-section measuring 2.625" x 3.0".

24
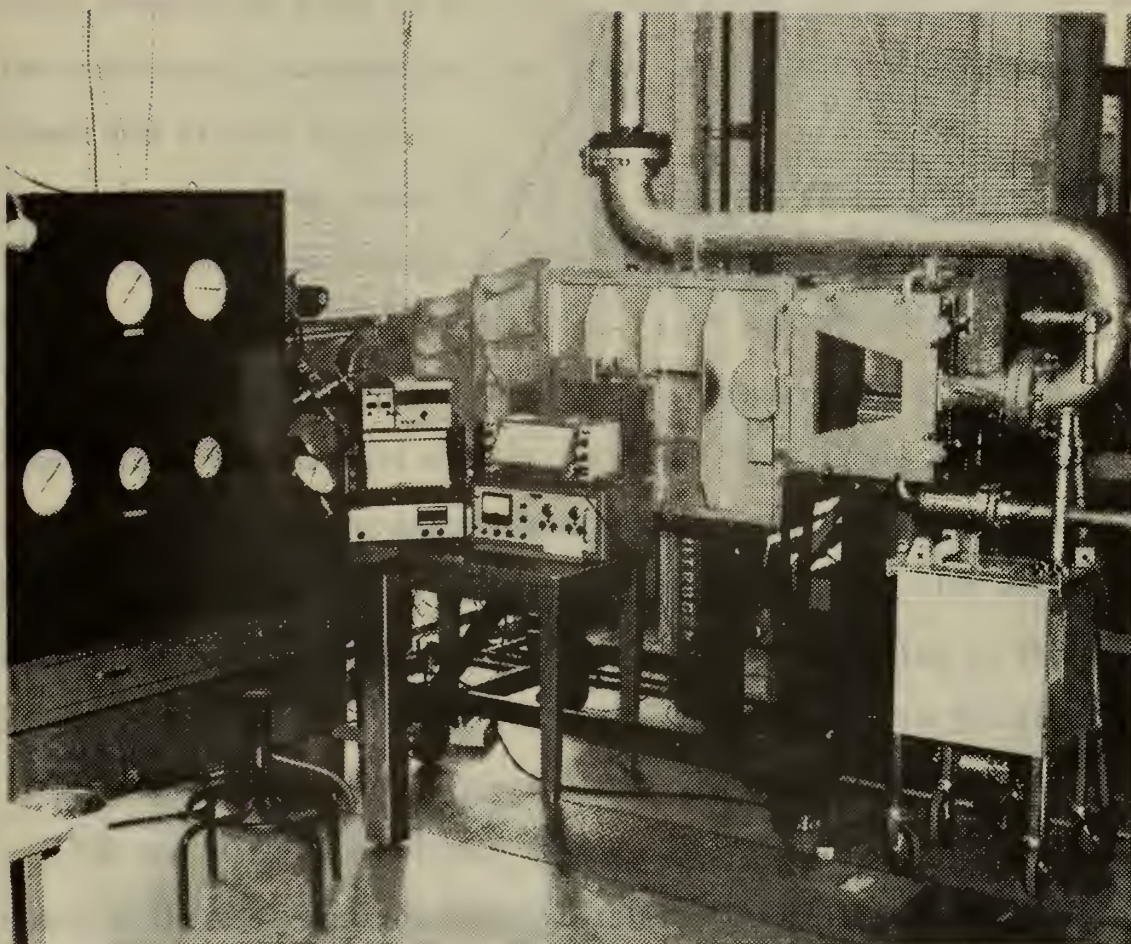
Figure 4. Primary Flow System with Control Panel.

The 5-inch pipe and subsequent transition section were part of a small
wind tunnel which had been obtained as surplus government equipment.
Since the available compressed air tanks could not provide sufficient
blow-down times through the existing cross-section, the test section
that was installed in the tunnel had plexiglass inserts on either side
which reduced the width of the tunnel from 2.625" to 1.4". In this way
the rectangular cross-section just prior to the test section had the
dimensions of 1.4" x 3.0".

The test section, shown in Fig. 5, consisted of a countoured upper
block and a flat lower block which contained the jet slot. The con-
toured upper block choked the flow at a 1.4" x 0.737" throat. The air
then exited through a nozzle which was divergent on one side only, the
upper block; the straight wall of the lower block served as a plane of
symmetry for simulating symmetric injection. The lower block was fitted
with variable inserts to allow for a change in both the slot width, d_t,
and the angle of injection α (see Fig. 6). Care was taken in the design
of the inserts to insure that the jet occupied the entire jet slot
(from side wall to side wall) upon entry into the mainstream flow.

The secondary flow followed a path similar to the primary system in
reaching the test section. Eight bottles of compressed nitrogen, mani-
folded together, provided the secondary flow. (See Fig. 7). After
leaving the manifold, the nitrogen passed through a remote controlled
pressure regulating valve. The regulator would reduce the 1800 psig
bottle pressure of the nitrogen to values ranging from 0 psig to 1500
psig. The nitrogen then flowed through a remote controlled on-off valve
and on through a section of 1" stainless steel tubing which was fitted
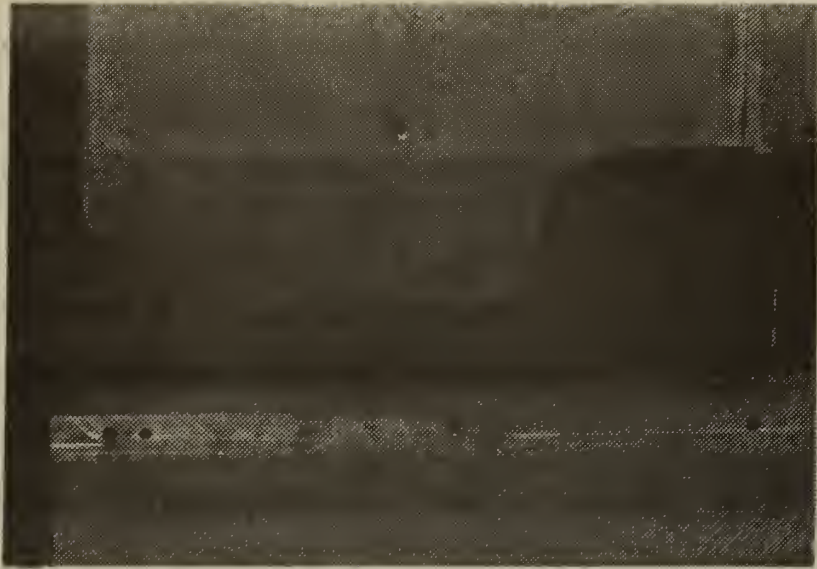
Figure 5.   Test Section
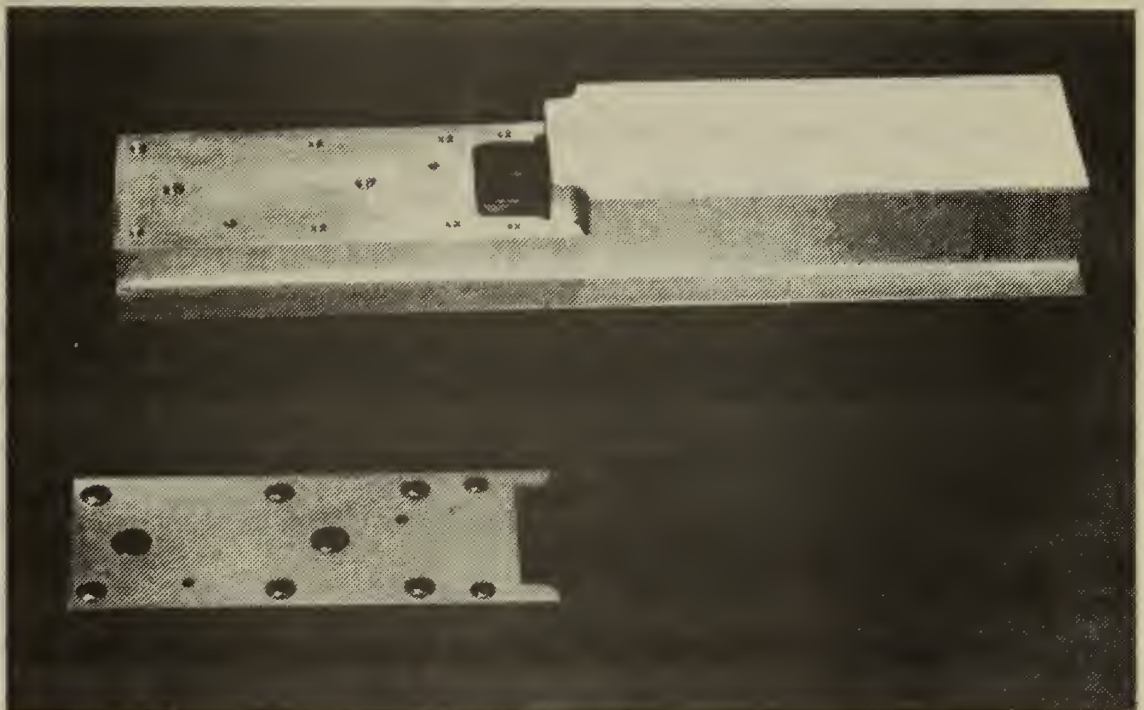
Figure 6.   Lower Block with Removeable Insert.

with a standard ASME flat plate orifice to a plenum chamber located in the lower block of the test section. From the plenum chamber the secondary flow was exhausted through a slot of variable width, and into the primary flow at the sonic throat.

The instrumentation for both the primary and secondary systems consisted of variable reluctance pressure transducers whose output was continuously recorded on strip chart recorders. In this way, the orifice pressure drops and corresponding upstream pressures required for determining mass flow rates by the ASME Power Test Code methods, [Ref. 18], as well as the total pressure measurements for both the primary and secondary system, were obtained as a continuous record during any experimental run. The total pressure probe for the primary system was mounted in the transition section just prior to the test section, and the total pressure probe for the secondary system was mounted in the plenum chamber in the lower block of the test section. Along with the output from the pressure transducers, bourden tube gages installed in a control panel, Fig 4, registered the total pressure of both systems, reservoir pressure of the primary system, and control pressure for the primary and secondary pressure regulating valves. The remote controls for the reducing valves as well as the on-off valves were also located on this control panel for convenience of operation.

The mainstream supply pressure, set at P_{mo}^{o} = 35.0 psig, was chosen for convenience and to provide sufficient run times. The flow of the unthrottled nozzle was measured for mainstream total pressures of 30.0 psig to 50.0 psig with an average discharge coefficient in the range of 1.05 ± .02. The discharge coefficient used here is defined to be the actual flow divided by the theoretically predicted flow. Considerable
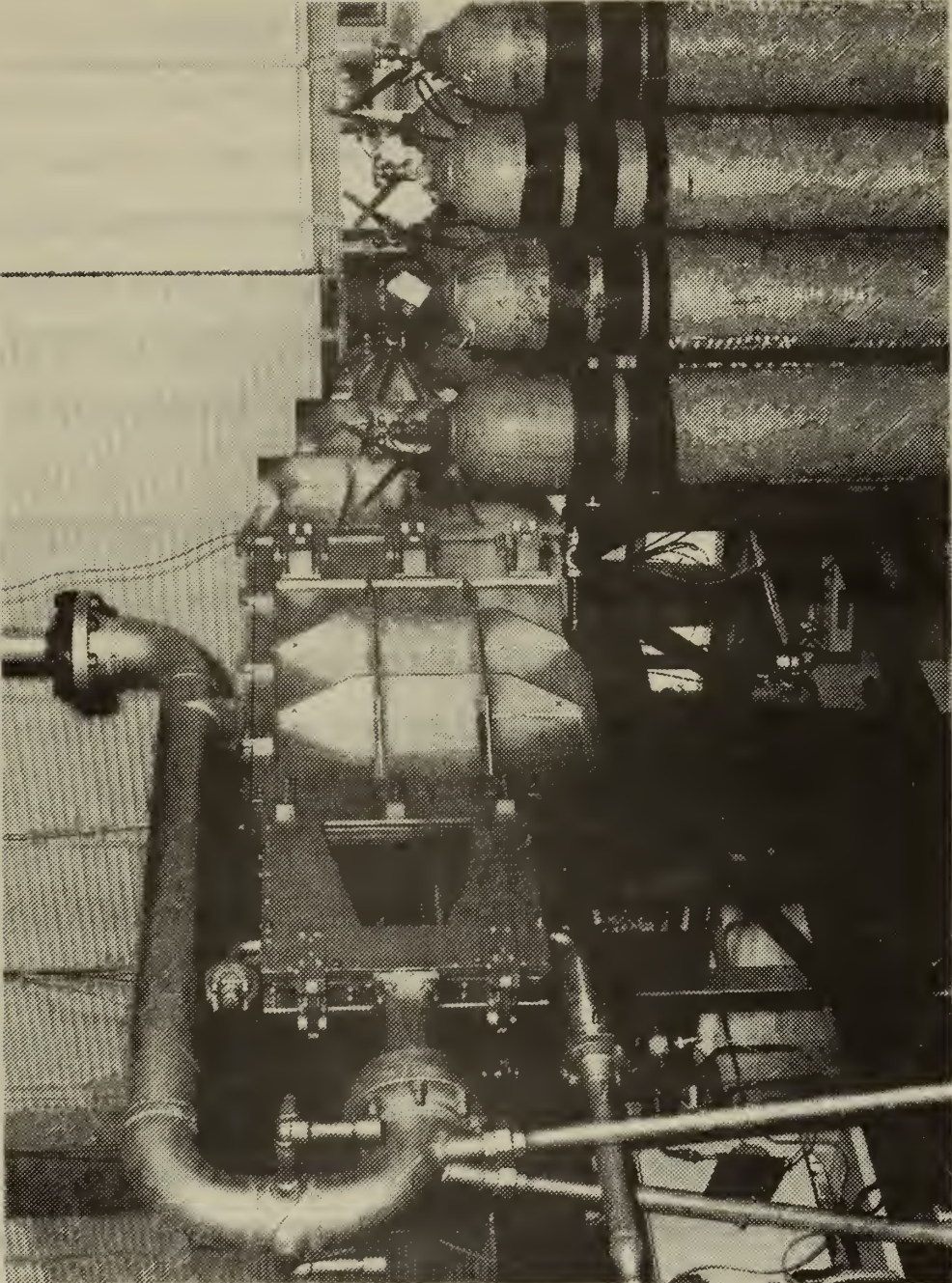
Figure 7. Secondary Flow System.

effort was expended to reduce the system leakages to a minimum value so
that all of the measured primary flow actually passed through the throat.
The value of the discharge coefficient given above indicates that this
effort was not completely successful but further reductions would have
entailed massive modifications to the equipment on hand. Further
comments concerning the difficulties with the experimental apparatus are
given in the section on recommendations for future work. At the supply
pressure of 35.0 psig and air temperature of 530°R the resulting mass
flow rate of the mainstream air was 1.19 lbm/sec. This value was used
for $\dot{m}_r$ in the reduction of data after correcting for slight variations
in P^O_{mo}.

The test section was provided with windows so that visual observations
of the jet/mainstream interaction could be made. Visual flow patterns
were obtained by coating the inside surfaces of the plexiglass inserts
with a mixture of titanium dioxide (TiO_2) and 200 Dow Corning Silicone
Oil with a viscosity of 350 centistokes.   The oil and titanium dioxide
were mixed in the proportions of 7cc of oil with 1cc of TiO_2. The
mixture was applied with a brush with little regard to the coating
thickness since the viscosity is the parameter which dictates the speed
which which the coating is blown off. Photographs were taken of the
resulting flow patterns. Although it is difficult to obtain any
quantitative results from these pictures, they were useful in
qualitatively examining the jet/mainstream interaction region.

A simplified linear error analysis was performed on the experimental
data in an attempt to arrive at bounds on the uncertainty of the mass
flow ratios of:

$$\frac{\dot{m}_m}{\dot{m}_r} \quad \text{and} \quad \frac{\dot{m}_j}{\dot{m}_r}.$$

The sources of error in the experimentally determined mass flow rates
fall into three main categories: the first being the error associated
with the various parameters which enter into the equation for determining
the mass flow rates from the ASME Power Test Code; the second is the
error in the pressure transducers and associated electronics; and, the
third is the error in reading the pressure traces on the strip chart
recorders.

The error associated with the various constants appearing in the
ASME mass flow rate equation was found to be insignificant. Furthermore,
when examining the error in the ratio of mass flow rates, i.e.,

$$\frac{\dot{m}_m}{\dot{m}_r} \, ,$$

it was found that any error in the previously mentioned quantities
would have no effect on the error of the ratio since the same error
appears in $\dot{m}_m$ and $\dot{m}_r$ and would therefore cancel out. The total error
in the ratio:

$$\frac{\dot{m}_m}{\dot{m}_r} \, ,$$

was found to be a function of the error in measuring the pressure drop
across the orifice plate, as well as in measuring the upstream static
pressure. Furthermore, the error in both of these pressure measurements
is dependent upon transducer error and reading error.

Each individual pressure transducer along with the associated
electronics and strip chart recorder was calibrated as a total unit. In
this way, much of the error which might have been inherent in single
components was calibrated out of the system. It is felt that the
transducers and electronics used for determining the upstream static

31

pressure and the total pressure for both the primary and secondary systems, were capable of determining the pressure to within ± 1.0 psi. Combining the transducer error with the error associated in reading the trace on the strip chart recorders, provided a measure of the total error in determining the upstream static pressure and total pressure of the flow. It was found that the static pressure and the total pressure of the primary and secondary systems could be determined to within ± 1.25 psi and ± 3.0 psi respectively. The sensitivity of the differential transducers used for measuring the pressure drop across the orifice plates was such that the differential pressures could be determined to within ± 0.1 psi. This value includes the error in reading the strip chart recorder. By using the previously determined errors for the individual pressure measurements, upper and lower bounds were determined for the uncertainty in the nondimensionalized ratios of:

$$\frac{\dot{m}_m}{\dot{m}_r} \quad \text{and} \quad \frac{\dot{m}_j}{\dot{m}_r} \; .$$

for:

$$\frac{\dot{m}_m}{\dot{m}_r} = 0.9$$

the percent uncertainty is ± 0.3 percent, and for:

$$\frac{\dot{m}_m}{\dot{m}_r} = 0.2$$

the percent uncertainty is ± 24.0 percent. The high error for the case of:

$$\frac{\dot{m}_m}{\dot{m}_r} = 0.2$$

(high throttling) comes from the measurement of the primary orifice

32

pressure drop. As previously mentioned, the total uncertainty in
measuring the pressure drop across the orifice plate was ± 0.1 psi. For
low values of:

$$\frac{\dot{m}_m}{\dot{m}_r}$$

(high throttling) the differential pressure is less than 0.5 psi, there-
fore the percent uncertainty in this measurement alone is on the order of
± 20.0 percent. This problem could be corrected if the flow measuring
device would give significantly larger pressure drops at the lower values
of:

$$\frac{\dot{m}_m}{\dot{m}_r} .$$

In the case of an orifice meter, this would entail using orifice plates
with smaller diameters as the throttling was increased. The experimental
setup for this study did not lend itself to changing the orifice plates
without considerable effort, so all experimental runs were conducted with
the same size orifice plate. It should be noted however, that the
consistency of the data seems to indicate that the data falls well within
the bounds of uncertainty. A similar analysis was performed for the
ratio:

$$\frac{\dot{m}_j}{\dot{m}_r}$$

and it was found that the percent uncertainty in this ratio was on the
order of ± 1.5 percent over the entire range of:

$$\frac{\dot{m}_j}{\dot{m}_r} .$$

Whereas the uncertainty is given for the ratio of mass flow rates, it must be remembered that the uncertainty for the primary or secondary mass flow rate alone, may differ significantly from the uncertainty for the nondimensionalized ratio. For example, if:

$$\frac{\dot{m}_m}{\dot{m}_r} = 0.484$$

the percent uncertainty in this ratio is ± 3.8 percent. However, the percent uncertainty in $\dot{m}_m$ alone is ±5.5 percent.

IV. DISCUSSION OF RESULTS

Throttling measurements were obtained for values of H of 0.02, 0.04 and 0.08 for perpendicular injection ($\alpha = 0°$). Measurements were also taken for $\alpha = 15°$ with H = 0.023, and $\alpha = 30°$ with H = 0.027. For each of these five settings the jet supply pressure was varied so that data were obtained for:

$$\frac{\dot{m}_j}{\dot{m}_r}$$

over a range of 0 to 0.6. Figures 8 and 9 show the results of the throttling measurements.

Examination of the data in Fig. 8 shows that although the data is consistent and repeatable, there is a general departure of the theory from the data. An improvement on the analytical model will be discussed in detail below.

In Fig. 9, it is evident that the effect of angle of injection as predicted by the theory is qualitatively verified. However, it appears that as the angle of injection exceeds approximately 30° the effect on the throttling becomes negligible. This phenomenon has also been observed by Nunn [Ref. 6]. At high angles of injection it is probable that the primary air flow partially fills the jet slot and the effective angle of injection becomes something less than the designed-for value. (See Fig. 10) The departure of the theory from the data at high angles of injection can be partially attributed to the fact that the analytical model fails to account for such phenomena.

The general departure of the theoretical curves from the data led to a re-evaluation of the analytical model. It is felt that the weakest
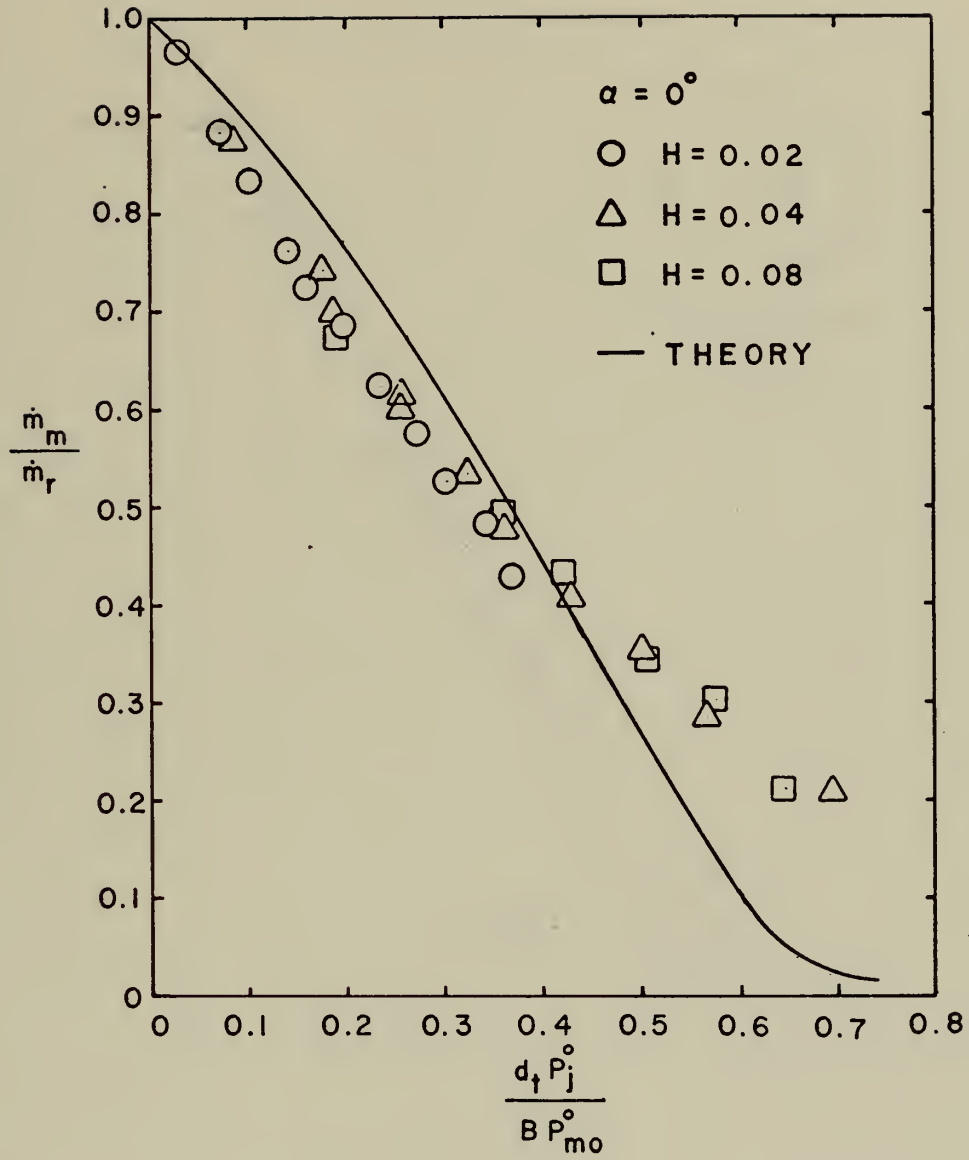
Figure 8. Throttling for Normal Injection (Unmodified Theory).
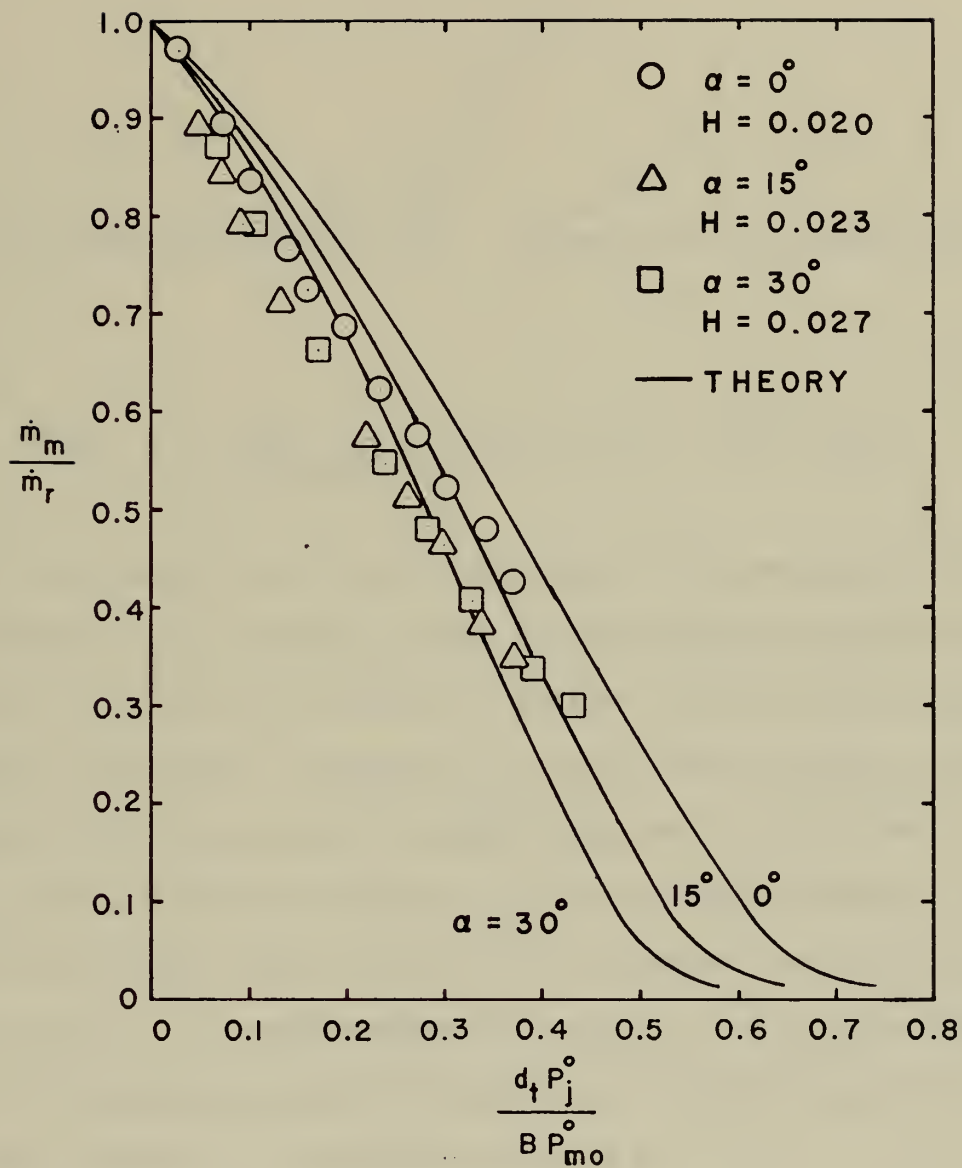
Figure 9. Throttling For Various Angles of
Injection (Unmodified Theory).
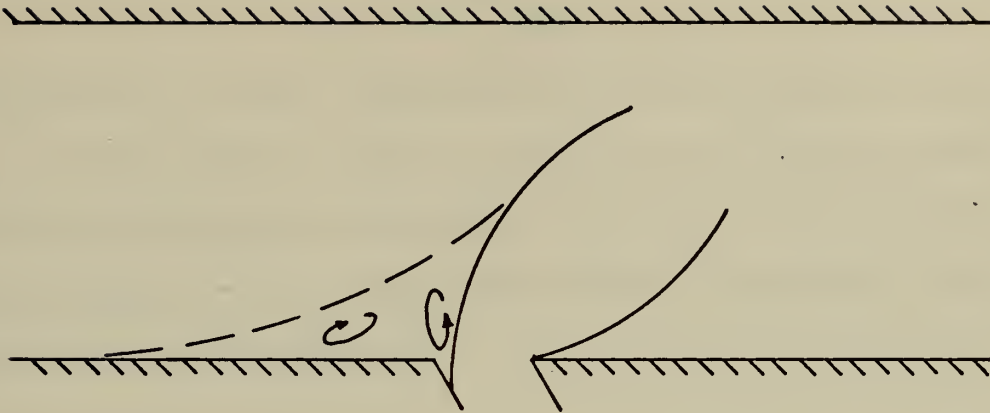
Figure 10. Effect of Mainstream on Jet at High Angles
of Injection.

part of the analysis is in the determination of the pressure acting on

the windward face of the jet by means of the assumption that the press-

ure varies from the static pressure at station 1 down to P_m^* at the point

of maximum penetration. Although P_m^* is fixed since the point of maximum

jet penetration is the point of minimum flow area for the primary fluid,

it can be argued that the pressure in the recirculatory region at the

base of the windward face of the jet may be greater than the mainstream

static pressure. A pressure weighting factor, β, was sought which would

allow for the mainstream total pressure to act of the windward face of

the jet at station 1. The following form of β:

$$\beta = \frac{P_{mo}^0}{P} - \left[\frac{P_{mo}^0}{P} - 1 \right] \left(\frac{y}{h} \right)^s , \qquad (14)$$

when substituted into Equation (6) satisfies the boundary conditions:

$$\beta P = P_{mo}^{o} \quad at \quad y = 0$$

$$\beta P = P \quad at \quad y = h$$

The effect of β is thus to weight the pressure distribution in such a
way as to yield higher pressures at the base of the windward face of the
jet while maintaining the condition $P = P_m^*$ at $y = h$. The effective
average pressure acting on the windward boundary of the jet is now
expressed with βP replacing P:

$$\frac{F_x}{h} = \frac{1}{h} \int_{y_1}^{y_2} \beta P \, dy \qquad (6a)$$

If, following previous developments, Equation (6a) is expressed in terms
of Mach number and substituted into Equation (5), an equation in terms
of the mainstream Mach number, M_{mo}, appears as follows:

$$\frac{d_t P_j^o}{BP_{mo}^o} = \frac{[A(M_{mo})]^{S-1}}{C[A(M_{mo})-1]^S} \int_{M_{mo}}^{1} \left[1 - \frac{A(M)}{A(M_{mo})} \right]^S \left[\frac{1}{M} - \frac{\frac{\gamma+1}{2} M}{1 + \frac{\gamma-1}{2}M^2} \right] \left[P(M) - 1 \right] dM$$

$$+ \frac{1}{C[A(M_{mo})]} \int_{M_{mo}}^{1} A(M) \left[\frac{1}{M} - \frac{\frac{\gamma+1}{2} M}{1 + \frac{\gamma-1}{2}M^2} \right] dM \qquad (10a)$$

where:

$$C = \left(\frac{2}{\gamma+1} \right)^{\frac{\gamma}{\gamma-1}} \left[\gamma (1 + \sin \alpha) + 1 \right]$$

Before Equation (10a) can be solved, a suitable value of s must be estimated. Figure (11) shows the dependency of β on s. It seems most probable that if a stagnation region exists at station 1, the mainstream stagnation pressure would act on the windward face of the jet over a short height (y very small) and decrease rapidly to the values calculated in the unmodified analysis. From this reasoning, a value of s<<1 would be the logical choice based on Fig. 11. The modified theoretical curve for $\alpha = 0°$ and s = 0.25 is shown in Fig. 12. Also shown in this figure is the unmodified theoretical curve and the theoretical curve from Nunn's analysis [Ref. 6]. The agreement between the data and the modified theory is extremely good up to $d_t P_j^o / BP_{mo}^o \approx 0.5$. For higher values of this parameter, the theory predicts greater throttling of the mainstream than was found experimentally.
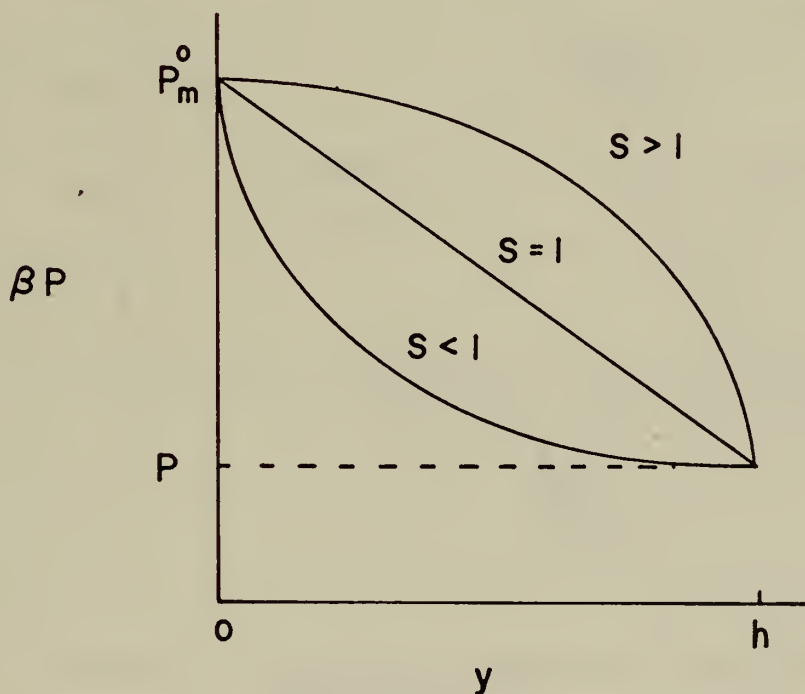
Figure 11. Effect of Exponent s on Pressure Weighting Factor, β.
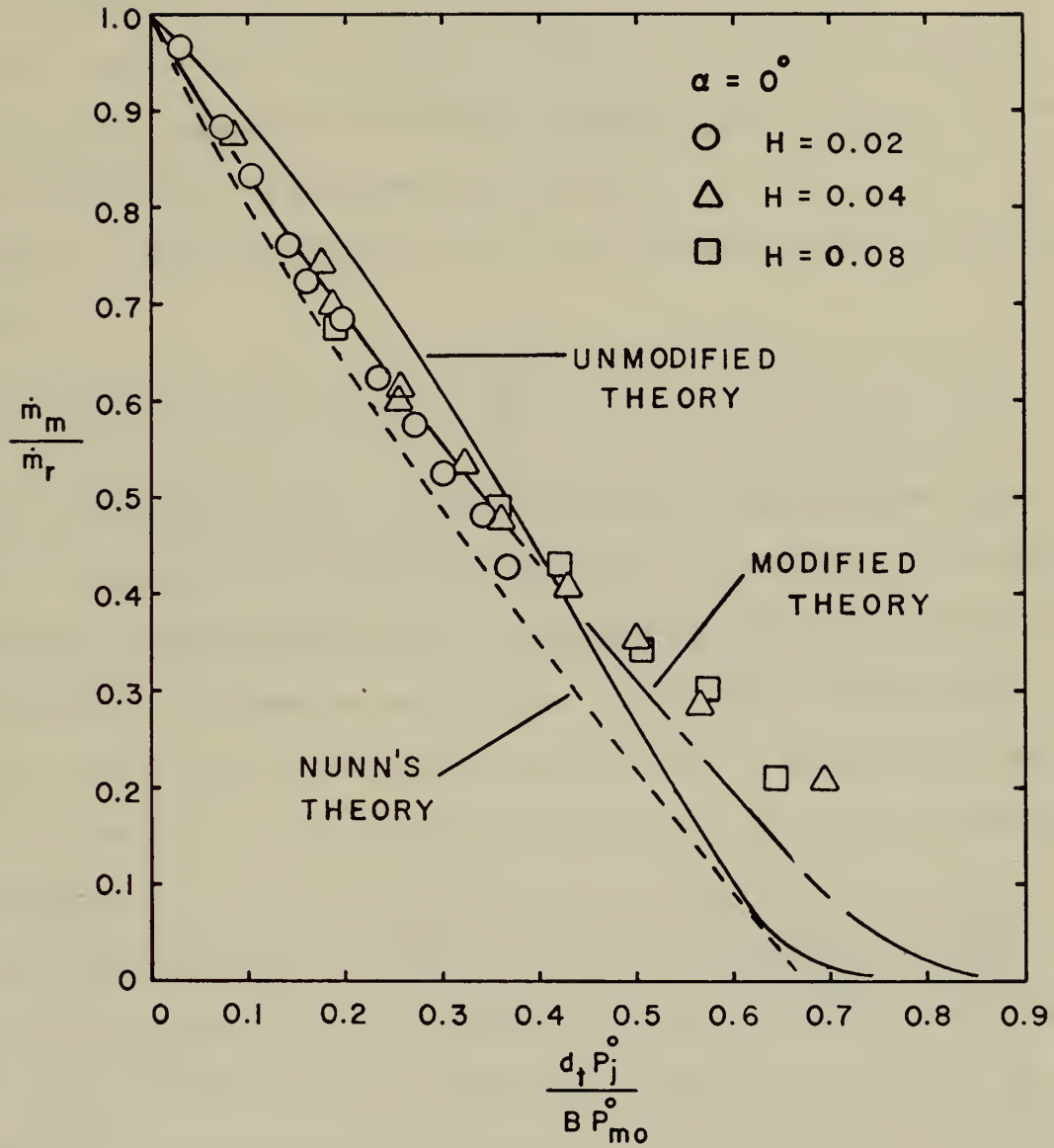
Figure 12. Comparison of Theoretical Curves for
Normal Injection.

It should be noted that Nunn's analysis predicts, for a given secondary flow, an improvement in the throttling of the primary flow as the slot width is reduced. The theory presented in this report does not predict such a dependence on slot width. Within the scatter of the data presented in Fig 12, it is felt that a dependency upon slot width, if any, is not clearly discernable. Further, it should be pointed out that Nunn's data included slot widths that were three times greater than the maximum slot width examined in this study.

Figure 13 shows a sequence of oil flow photographs taken for various values of:

$$\frac{P_j^O}{P_{mo}^O}$$

with $d_t = 0.059$ and $\alpha = 0°$. All three photographs exhibit the "Mach-bottle" characteristic of underexpanded jets as is expected. The photographs show very good definition of the windward boundary of the jet up to the point of maximum jet penetration. This lends a considerable amount of confidence to the assumption that there is a negligible amount of mixing between the jet and mainstream prior to the point of maximum penetration.

The shock pattern within the jet plume is not readily discernable from the photographs. It can probably be stated, however, that the Mach disk occurs somewhere close to the point of maximum penetration. It is clearly evident from the photographs that the jet reattaches itself to the wall after the point of maximum penetration. At the reattachment point the mark of an oblique shock can be seen coming off from the lower surface. This shock serves to curve the jet fluid back so that it again flows parallel to the lower block of the test section.

42

(a) $\dfrac{d_t P_j^0}{BP_{mo}^0} = 0.504$

(b) $\dfrac{d_t P_j^0}{BP_{mo}^0} = 0.65$
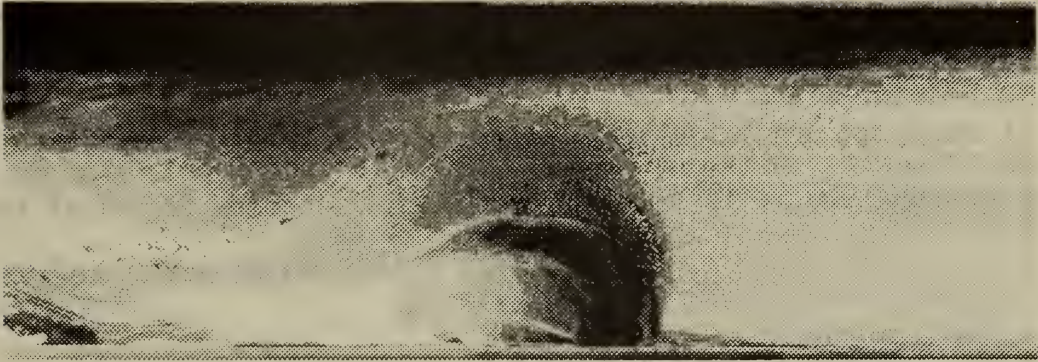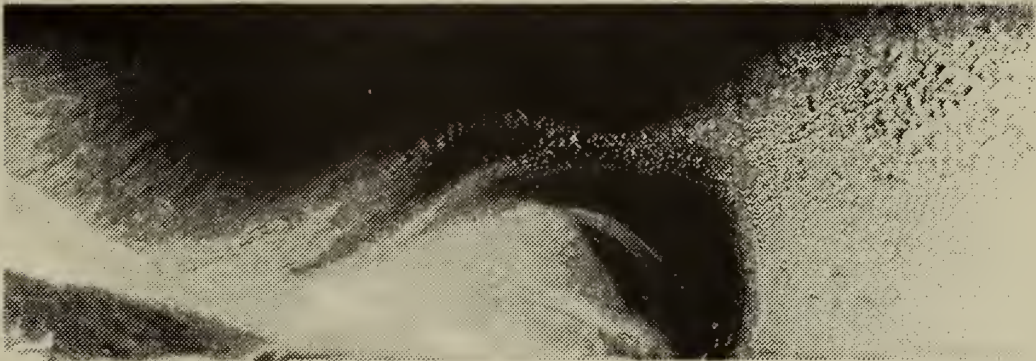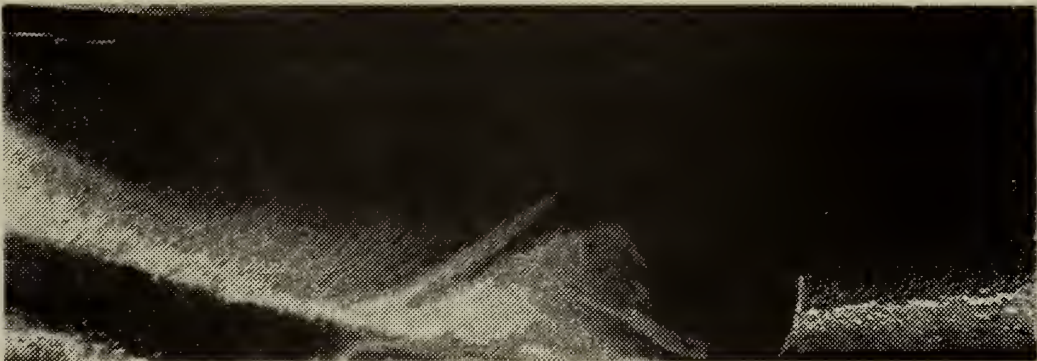
(c) $\dfrac{d_t P_m^0}{BP_{mo}^0} = 0.80$

Figure 13. Oil Flow Photographs, $d_t = 0.059$, $\alpha = 0°$.

43

Examination of the oil streaks on the surface of the lower block of the test section indicated that a small amount of the mainstream fluid flowed around the sides of the jet sheet thereby creating a three-dimensional problem rather than the hoped for two-dimensional situation.

The oil streak which appears in the interior of the jet plume is thought to be oil which is introduced into the jet at the sides by the recirculatory flow in the bubble region.

V. CONCLUSIONS

1. The important parameters in the process of throttling a sonic flow by the injection of a transverse jet, are the jet slot width (d_t), the angle of injection (α), and the ratio of jet to mainstream total pressures.

2. The sum $\dot{m}_m + \dot{m}_j$ is the controlling factor in determining the effectiveness of the throttling process and not $\dot{m}_m$ alone, since the secondary fluid, introduced for the purpose of throttling, contributes to the overall flow through the nozzle. A practical limit to the throttling process is around 60 percent reduction of the mainstream flow. Reduction of the mainstream beyond this level requires an increase in the secondary flow which is greater than the additional throttling achieved in the mainstream. For example, for normal injection, it requires a jet mass flow rate of approximately 40 percent of the mainstream reference flow to throttle the mainstream by 60 percent. The best overall throttling of a nozzle flow that can be attained is therefore approximately a 20 percent reduction when the sum of $\dot{m}_m$ and $\dot{m}_j$ is considered. Figure 14 shows the net throttling attainable ($\dot{m}_m + \dot{m}_j$) based upon the modified analytical model.

3. Within the range of parameters investigated here, the analytical model which includes the pressure weighting factor, β, with a value of $s = 0.25$, is adequate to predict the mainstream throttling up to the 60 percent level.

4. To achieve the maximum reduction in mainstream flow for a given level of secondary flow, the angle of injection should be a maximum. However,

45
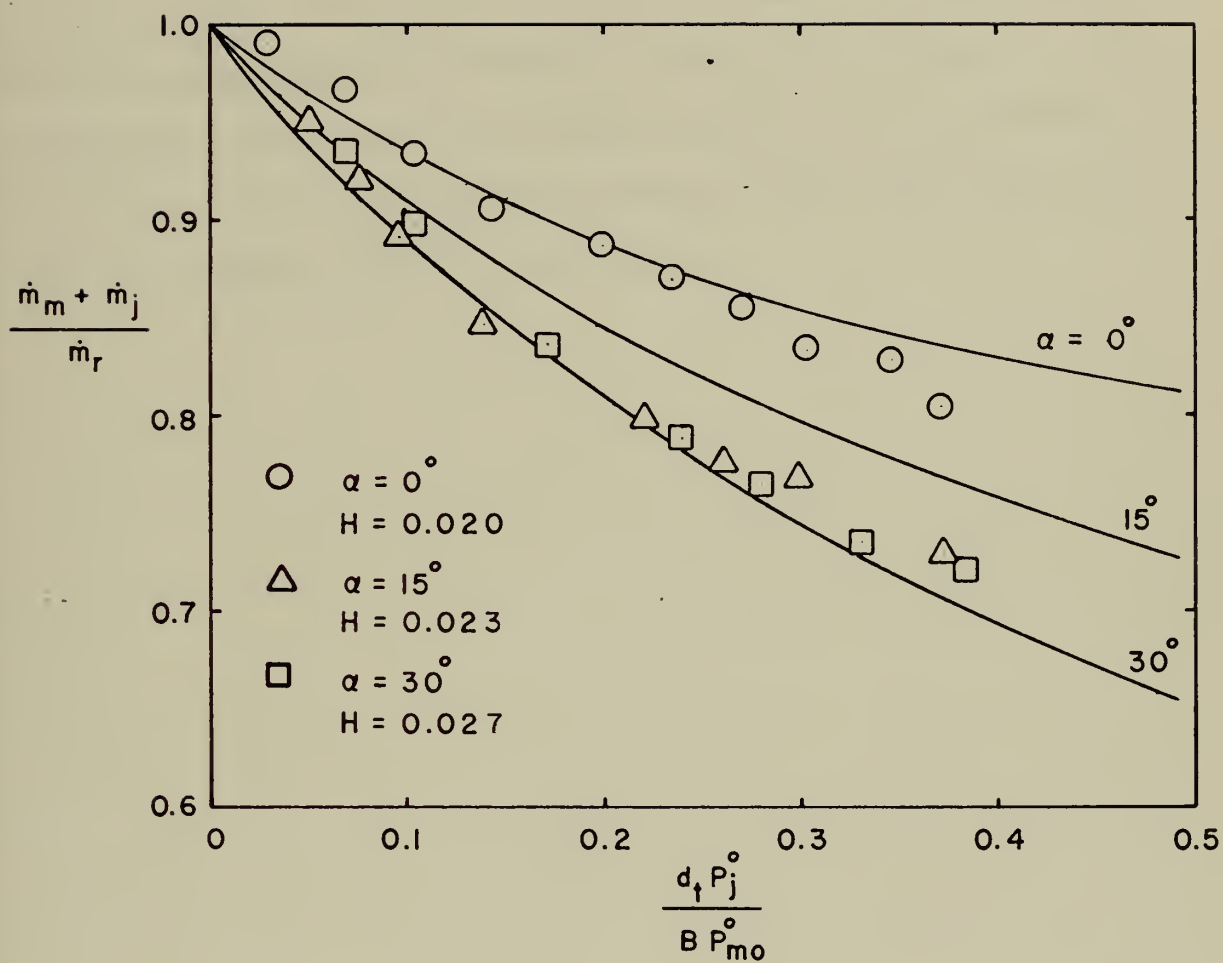
Figure 14. Net Throttling Available for Various Angles of Injection.

an increase in the angle of injection beyond 30° does not appear to appreciably increase the throttling effectiveness.

5. If jet throttling were used in a proportional amplifier/moment producer, the savings in gas expenditure during the no-control phase, would be offset by the increase in gas used during the control phase since one of the control jets would be on at all times. It is concluded that the use of aerodynamic throttling in fluidic control elements is not advantageous unless sufficiently higher throttling can be achieved with less secondary flow. Suggestions concerning future work towards this goal are included in the following section.

VI. RECOMMENDATIONS

1. Further study of the throttling process is warrented with regard to the effect of the jet slot width. Nunn's analysis [Ref. 8] predicts an increase in throttling with a decrease in the slot width, while the analysis presented here shows no such dependence on slot width. The data in both studies seemed to substantiate the theory presented for the analytical model in question.

2. The analytical model presented here will accurately predict the throttling for values of:

$$\frac{\dot{m}_j}{\dot{m}_r} < 0.5 \quad .$$

Further work should be done both experimentally and analytically to better understand the throttling process at values of:

$$\frac{\dot{m}_j}{\dot{m}_r} > 0.5 \quad .$$

3. Further work should be done with regard to the effect of high angles of injection on the throttling process. First, an analytical model is needed which would account for the fact that the effective angle of injection, as seen by the primary flow, is often less than the designed for angle of injection. Secondly, an experimental setup is needed that would allow for angles of injection approaching 90° with some confidence that the angle of injection, as designed into the experimental setup, will be felt by the primary flow.

4. Regarding the experimental apparatus used for this study, it is recommended that if it is desired to use this equipment for future

throttling studies, major modifications be made. It is recommended that
the wind tunnel be discarded and that an entirely new test section be
designed that would mount directly to the transition section from the
5" pipe to the present test section. In this way, the need for reducing
the width of the tunnel by use of inserts could be eliminated and a
noticeable improvement in the discharge coefficient should be realized.
It should be mentioned again that the differential pressure measurement
required for determining the mass flow rate when using an orifice meter
was a major source of error. If orifice meters are used in future work,
it is recommended that they be installed such that the orifice plates
could be easily changed so that a reasonable pressure drop would be
measured for all levels of throttling. It is further recommended that
alternative methods of determining the mass flow rates of the primary
and secondary systems be sought. Finally, a high pressure compressor
and air receivers should be obtained to provide for the secondary flow
system. Although the present system has operated quite well, the high
expenditure of Nitrogen has made data gathering an expensive proposition.

The method of characteristics (MOC) is a well known numerical method for obtaining the solution of the complete differential equations of motion for supersonic, two-dimensional flow. There are two basic methods which use the MOC in analyzing a particular flow field; the Lattice method, and the Field method. The field method was used in this study, however, a brief description of both methods is included for comparative purposes. Both methods assume that the ratio of specific heats is constant and that the flow is isentropic, inviscid, and irrotational.

A. LATTICE METHOD

In the lattice method, the calculation of flow properties progresses from a known data line along right and left-running characteristics. The flow properties ν and θ behave in a special way along characteristics:

$$\nu + \theta = \text{constant} \qquad \text{right-running}$$

$$\nu - \theta = \text{constant} \qquad \text{left-running}$$

If ν and θ are known along some data curve, then the values of ν_p and θ_p at some point P can be determined from Equations (A-1) and (A-2). (See Fig. A-1-a.)

$$\nu_p = \frac{1}{2} (\nu_1 + \nu_2) + \frac{1}{2} (\theta_1 - \theta_2) \qquad\qquad \text{(A-1)}$$

$$\theta_p = \frac{1}{2} (\nu_1 - \nu_2) + \frac{1}{2} (\theta_1 + \theta_2) \qquad\qquad \text{(A-2)}$$

Once the values for ν and θ at point P are found, the other flow parameters are easily found. It still remains, however, to locate point P.
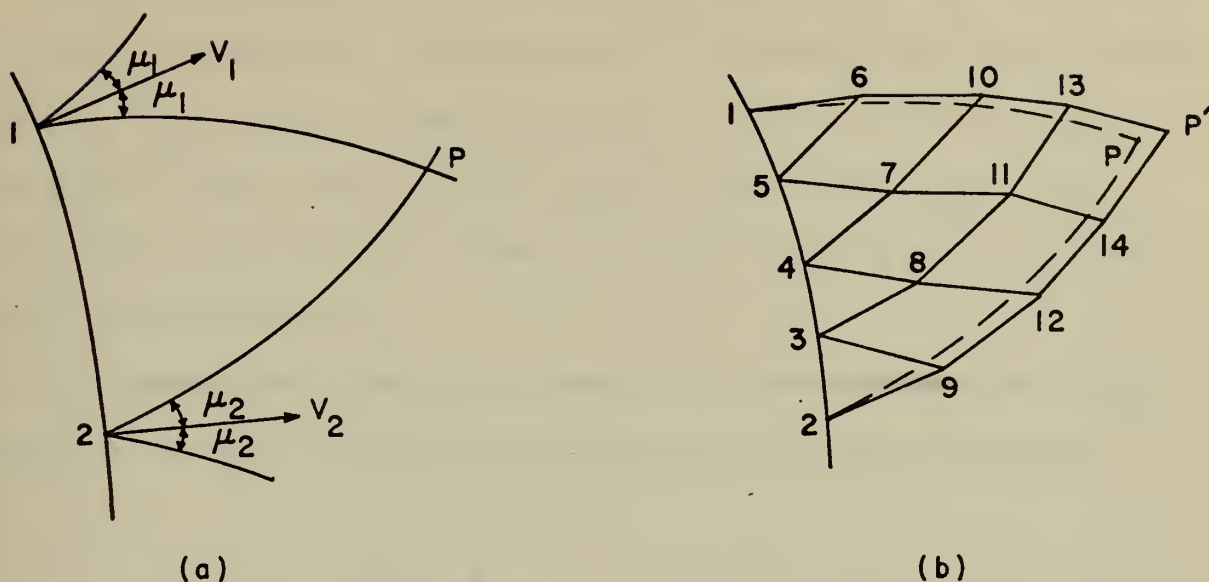
Figure A-1. Lattice Method.

The characteristics at point 1 make an angle μ_1 with the flow direction; but if the Mach number changes as the flow progresses downstream, the angle μ changes and the characteristic lines become curved. The curved characteristics are approximated by straight lines or a series of straight lines as shown in Figure A-1-b. As the mesh size is reduced and more intermediate points are used in locating point P, the accuracy of the problem is increased.

B. FIELD METHOD

At any boundary change or other flow disturbance, waves are formed, and if these waves are weak, they may be used in a manner similar to characteristics. It must be remembered, however, that when using weak waves as characteristics, the flow properties are discontinuous across the wave.

In a region bounded by waves, the flow properties are constant. As a wave is crossed and a new region (cell) is entered, the flow properties change to new values but remain constant in the new cell. The waves divide the total flow field into cells of uniform flow. Thus, the calculation of properties in the flow field progresses from a reference cell to adjoining cells.

Figure A-2 shows how the jet plume for an underexpanded sonic nozzle would be divided into cells by the expansion and compression waves.
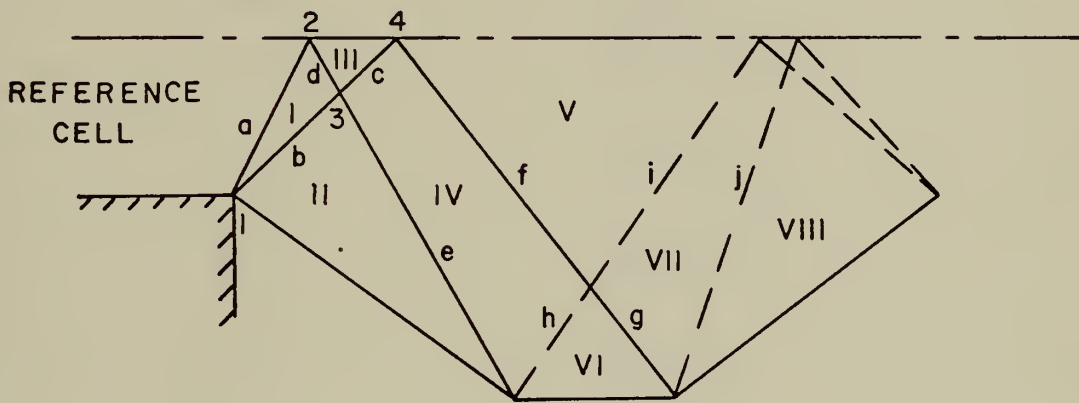
Figure A-2. Field Method.

Expansion Waves - a,b,c,d,e,f,g
Compression Waves - h,i,j
Roman numerals - Cell numbers

All waves are assumed to be of equal strength such that they all deflect the flow the same amount δ. Expansion waves from the lower boundary (a,b, and c) turn the flow away from the center-line by amount δ and the expansion waves from the upper boundary (d,e,f, and g) as well as the compression waves from the lower boundary (h,i, and j) turn the flow back toward the center-line by amount δ. Rotty [Ref. 19] suggests that the cells be identified by four numbers $\begin{pmatrix} m & o \\ n & p \end{pmatrix}$; m indicates the

number of expansion waves generated at the upper boundary that must be crossed in reaching the cell, n indicates the number of expansion waves originating at the lower boundary which must be crossed, o the number of compression waves from the upper boundary, and p the number of compression waves from the lower boundary which must be crossed to reach the cell in question. Table A-I shows how the cells in Fig A-2 would be identified:

Table A-I. Cell Identification.

CELL	$\begin{pmatrix} m & o \\ n & p \end{pmatrix}$
REF.	$\begin{pmatrix} 0 & 0 \\ 0 & 0 \end{pmatrix}$
I	$\begin{pmatrix} 0 & 0 \\ 1 & 0 \end{pmatrix}$
II	$\begin{pmatrix} 0 & 0 \\ 2 & 0 \end{pmatrix}$
III	$\begin{pmatrix} 1 & 0 \\ 1 & 0 \end{pmatrix}$
IV	$\begin{pmatrix} 1 & 0 \\ 2 & 0 \end{pmatrix}$
V	$\begin{pmatrix} 2 & 0 \\ 2 & 0 \end{pmatrix}$
VI	$\begin{pmatrix} 1 & 0 \\ 2 & 1 \end{pmatrix}$
VII	$\begin{pmatrix} 2 & 0 \\ 2 & 1 \end{pmatrix}$
VIII	$\begin{pmatrix} 2 & 0 \\ 2 & 2 \end{pmatrix}$

If the values for v_R and θ_R are known in the reference cell, then the values for v and θ can be found in any other cell from the four identifying numbers m,n,o, and p.

$$v = v_R + \delta(m + n - o - p) \qquad (A-4)$$

$$\theta = \theta_R + \delta(m - n - o + p) \qquad (A-5)$$

After the flow properties v and θ are known throughout the flow field, it becomes necessary to determine the locations of the wave intersections so that the flow field can be accurately mapped. To locate the wave intersections it must be remembered that the waves are assumed to be characteristics and, as such, they make an angle μ with the local flow direction θ. The problem now becomes one of finding the directions of the right and left-running characteristics for each cell in the flow field. The Mach number in the cell can be found from the Prandtl-Meyer expression:

$$v(M) = \sqrt{\frac{\gamma+1}{\gamma-1}} \ \text{TAN}^{-1} \sqrt{\frac{\gamma-1}{\gamma+1}(M^2 - 1)} - \text{TAN}^{-1} \sqrt{M^2 - 1} \qquad (A-6)$$

The Mach angle, μ, is found from:

$$\mu = \text{SIN}^{-1} \frac{1}{M} \qquad (A-7)$$

and the directions of the characteristics for a given cell are:

$$\theta - \mu \qquad \text{right-running} \qquad (A-8)$$

$$\theta + \mu \qquad \text{left-running} \qquad (A-9)$$

The directions of the waves in Fig. A-2 are calculated in the following manner. The direction of wave (a) is assumed to be an average of the left-running characteristics in the reference cell and cell I.

Similarly the direction of wave (d) is found from averaging the values of the right-running characteristics in cells I and III. In this manner, the directions of all waves can be calculated. Locating point 2 in Fig. A-2 is now a simple matter since point 1 and the vertical distance from point 1 to the center-line are prescribed, and the direction of wave (a) is known. Similarly, with the location of point 2 known along with the directions of waves (b) and (d), the location of point 3 can be determined. The calculation of additional points proceeds in an orderly fashion from already calculated points along waves whose directions are known.

The accuracy of this method depends on the number of expansion waves that are chosen for the initial expansion fan at the nozzle lip.

The first step in analyzing the flow field for a free jet is to determine the initial expansion of the flow at the nozzle lip. The flow angle, $\Delta\nu$, through which the flow will expand is the difference between the Prandtl-Meyer expansion angles corresponding to the nozzle-exit Mach number (ν_N) and the jet-boundary Mach number (ν_B). Inclusion of the flow direction as imparted by the nozzle half-angle θ_N completes the equation for finding the initial turning angle:

$$\beta = \nu_N - \nu_B - \theta_N \qquad\qquad (A-10)$$

This study restricted itself to jets which were sonic at the nozzle exit and had a nozzle half-angle equal to zero, therefore Equation (A-10) becomes:

$$\beta = -\nu_B$$

The initial turning angle β is equal to the flow direction in cell II in Fig. A-2. The boundary Mach number, the only unknown in determining

ν_B, is a function of the ambient pressure P_∞, and the jet total pressure P^0_j, and can be found from the isentropic pressure relationship:

$$\frac{P_\infty}{P^0_j} = \left(1 + \frac{\gamma-1}{2} M^2\right)^{\frac{\gamma}{1-\gamma}} \qquad (A-12)$$

Using the Prandtl-Meyer relationship, as given in Equation (A-6), ν_B can be determined.

The initial expansion fan at the nozzle lip, which turns the flow through angle β, is approximated by a finite number of N expansion waves. Thus, the strength, or flow deflection, δ, caused by one wave is:

$$\delta = \frac{\beta}{N} \qquad . \qquad (A-13)$$

As mentioned earlier, the accuracy of the field method improves as N is increased thereby decreasing the effect of any one wave.

C. APPLICATION OF FIELD METHOD TO FREE JET STUDY

The field method of the MOC was employed to determine the plume boundary of a jet issuing from a two-dimensional slot into a quiescent atmosphere. Since this calculation done by hand with any degree of accuracy would be a lengthy and time consuming process, a digital computer solution was used.

The computer program presented in this appendix was designed for use in the IBM 360/FORTRAN IV system installed at the Naval Postgraduate School.

In the discussion which follows, all procedures are set up for calculations below the center-line. Field coordinates are established with respect to an origin located on the center-line at the nozzle exit plane. The coordinates are given relative to one-half the width of the

56

nozzle exit; for example, the coordinates of the lower nozzle lip are: x = 0.0 and y = -1.0. The computer program maps the flow field downstream of the nozzle to a point where the effect of the first compression wave from the upper boundary is felt. Calculations do not proceed beyond this compression point. The decision to terminate the program at this point was based on the fact that the maximum width of the jet plume will occur prior to this point in the flow field. The location of maximum plume width is of special interest in this investigation since it has been shown by Vick, et.al. [Ref. 12] that the Mach disk occurs close to this point. The flow properties undergo a discontinuous change as the jet fluid passes through the Mach disk. The MOC will not predict the location of the Mach disk, nor will it consider the effect of the Mach disk on the downstream fluid. Therefore, further application of the MOC downstream of the Mach disk will not give accurate results.

The only inputs that are required for the program are the pressure ratio:

$$\frac{P^O_j}{P^O_\infty} \quad ,$$

and N the number of waves chosen for the expansion fan at the nozzle lip. The program assumes that the ratio of specific heats is equal to 1.4.

The first part of the program calculates the boundary Mach number, the initial turning angle (FTHETA), and the strength of each wave (DELTA). Based on the value of N, the total number of cells in the flow field (NC) is calculated along with another field parameter NOC. NOC is the cell number for which no compression waves have been encountered in reaching the cells numbering from 1 to NOC. Figure A-3 shows the cell numbering for a flow field with N = 4.
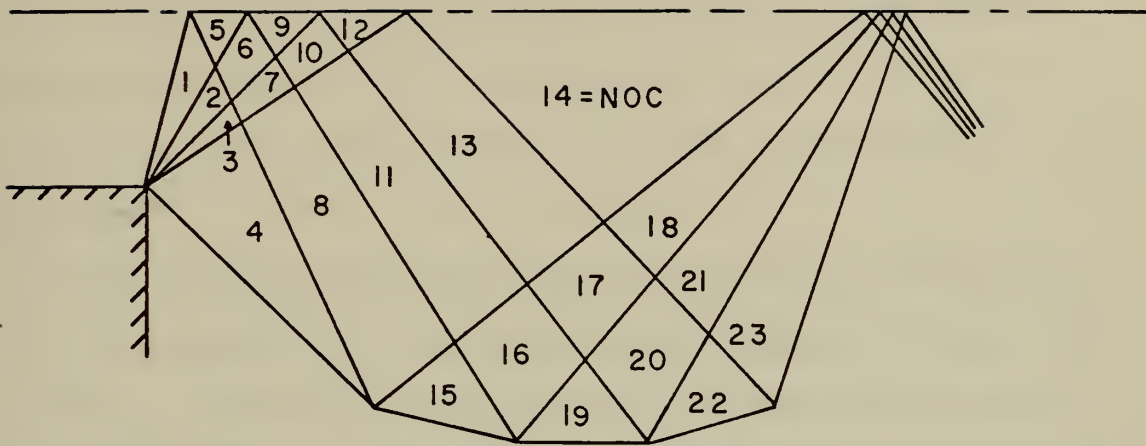
Figure A-3. Cell Numbering.

Since the program does not treat the flow field beyond the first
compression wave from the upper boundary, Equations (A-4) and (A-5)
appear as:

$$\nu = \delta(m + n - p) \qquad (A-14)$$
$$\theta = \delta(m - n + p)$$

The above expressions are valid only for a jet which is sonic at the
nozzle exit ($\nu_R = 0.0$), and with the nozzle half-angle equal to zero
($\theta_R = 0°$). Equations (A-14) and (A-15) appear in the program as:

$$V = DELTA(UE + LE - LC)$$
$$THETA = DELTA(UE - LE + LC)$$

where UE is the number of expansion waves from the upper boundary which
are crossed, LE is the number of expansion waves from the lower boundary
which are crossed, and LC is the number of compression waves from the
lower boundary which are crossed in reaching the cell in question.

58

The following six sections of the program assign the appropriate values of LE, UE, and LC to each cell, and then calculate ν and θ for each cell. After the program has calculated ν and θ Equation (A-6) is solved iteratively for the Mach number in each cell. With the Mach number known, the Mach angle μ, and the directions of the left and right-running characteristics can be calculated by using Equations (A-7) through (A-9).

At this point the program has stored all necessary information to locate the intersections of the expansion and compression waves. The intersections of the expansion waves with their own reflections from the center-line and the intersections of the expansion waves with the center-line are calculated first. Figure A-4 shows the numbering scheme for the intersections just mentioned.
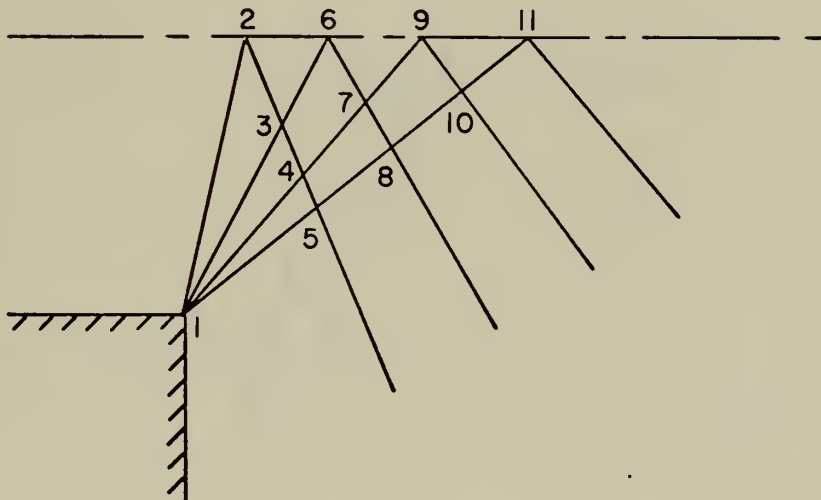
Figure A-4. Numbering Intersections of Expansion Waves.

The location of the wave intersections is carried out in the program in the same order as the intersections are numbered. As already mentioned, this section of the program locates two different types of intersections: expansion waves with the center-line; and expansion waves with their own reflections. Each type of intersection requires a slightly different procedure for locating the point of intersection. To begin with, two angles, A and B, are defined for the flow field. A is the angle that the waves from the lower boundary make with the center-line direction, and B is the angle that the waves from the upper boundary make with the center-line direction. Angle A is determined by averaging the directions for the left-running characteristics on either side of the wave in question. Similarly, angle B is found by averaging the directions of the right-running characteristics. Figure A-5 illustrates the method for locating an interior point such as point 3.
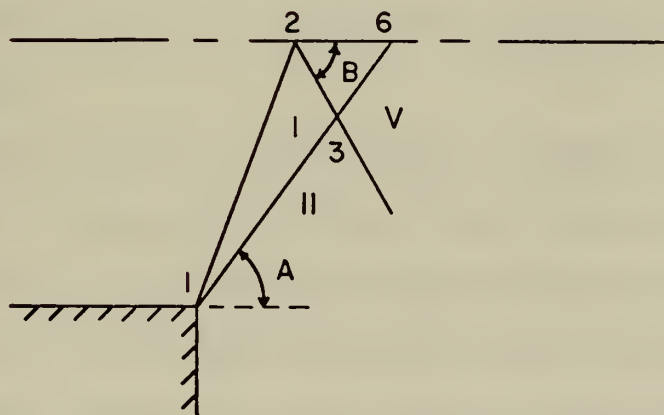
Figure A-5. Locating Interior Point.

60

Angles A and B are found and then expressed in terms of their tangents:

$$A = \frac{LR(I) + LR(II)}{2}$$

$$B = \frac{RR(I) + RR(V)}{2}$$

$$TAN\ A\ =\ \frac{y_3 - y_1}{x_3 - x_1} \qquad\qquad\qquad (A\text{-}16)$$

$$TAN\ B\ =\ \frac{y_3 - y_2}{x_3 - x_2} \qquad\qquad\qquad (A\text{-}17)$$

Solving Equations (A-16) and (A-17) for the unknowns, x_3 and y_3, yields:

$$x_3\ =\ \frac{y_2 - y_1 + x_1\ TAN\ A - x_2\ TAN\ B}{TAN\ A\ -\ TAN\ B} \qquad\qquad (A\text{-}18)$$

$$y_3\ =\ (x_3 - x_2)\ TAN\ B + y_2 \qquad\qquad\qquad (A\text{-}19)$$

Equations (A-18) and (A-19) may be used for locating any interior point
in the flow field simply by using the appropriate subscripts. With the
location of point 3 known, the center-line point (6) can be found as
shown in Fig. A-6.

By using the procedures just described, all center-line points and
interior points in the expansion region of the flow field can be found.

The next section of the program locates the intersections of the
expansion waves with the compression waves and the jet boundary. A new
numbering scheme is employed for this section of the program. (See
Fig. A-7.) The previously located intersections along the last expansion
wave from the nozzle lip are renumbered from 1 to N + 1 and then the
numbering continues along the compression waves.
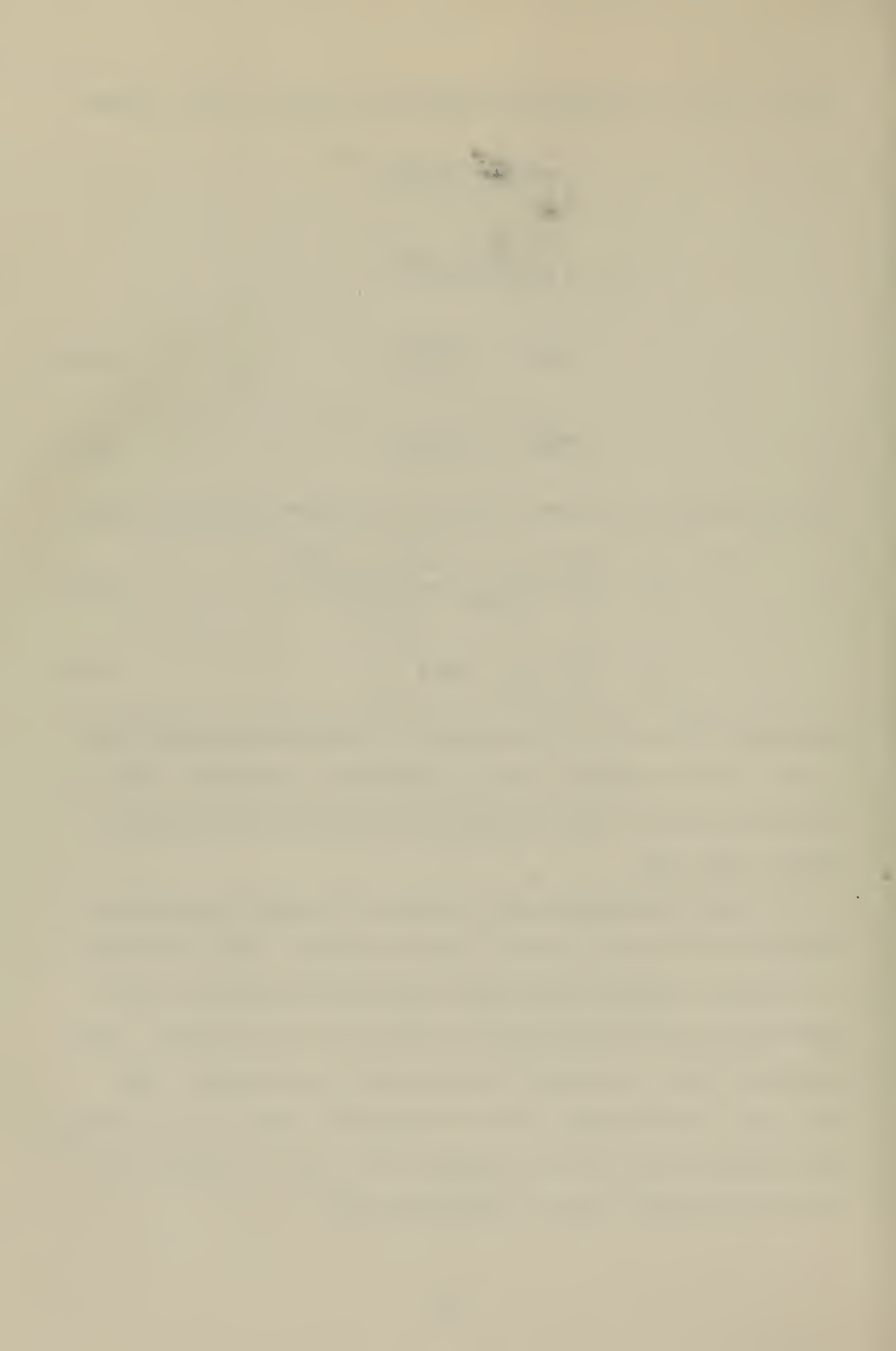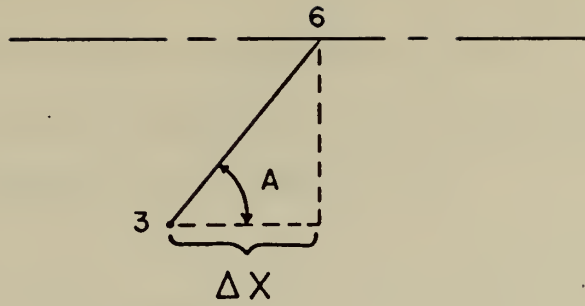
$$\Delta X = \frac{y_3}{TAN\ A}$$

$$X_6 = x_3 + \Delta X$$

$$y_6 = 0.0$$

Figure A-6. Locating Center-Line Point.
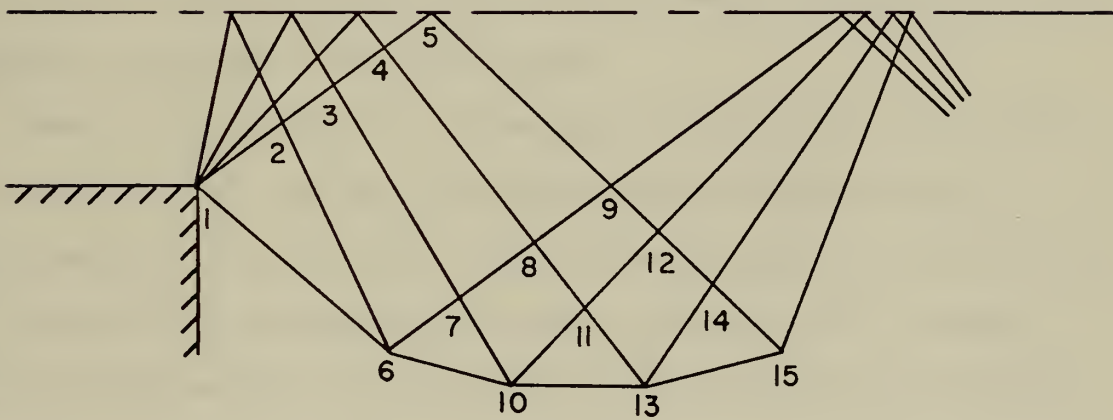
Figure A-7. Numbering Intersections of
Expansion/Compression Waves.

Locating the interior points in the compression region is done in the same way as in the expansion region, using Equations (A-18) and (A-19). The only change that need be made is in determining the value for angle A when locating a boundary point, see Fig. A-8.
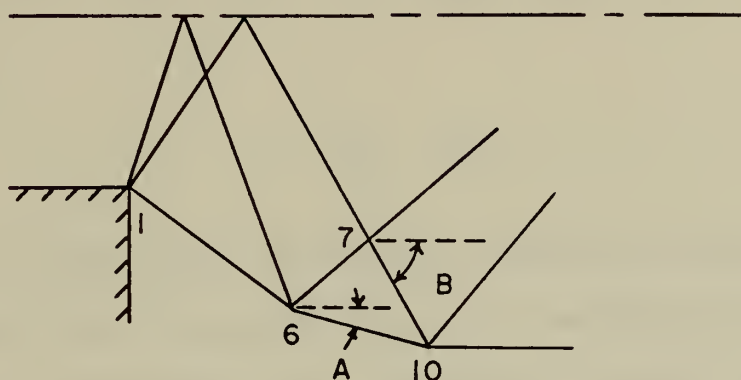
Figure A-8. Locating Boundary Point.

For this case, angle A is the same as the flow direction θ for the cell in question. By calculating angle A in this manner for boundary points, Equations (A-18) and (A-19) can be used.

There are two sections to the output from this program. The first is a listing of all the cells in the flow field along with their corresponding values of LE, UE, LC, θ, ν, Mach number, μ, and directions of right and left-running characteristics (RR) and (LR). The other section of the output is a listing of the calcualted points along the boundary of the jet plume. The boundary points are nondimensionalized with respect to the slot width of the jet.

As was mentioned previously, the MOC will not give accurate results downstream of the Mach disk. Since it has been shown that the Mach disk occurs close to the point of maximum plume width, it is felt that the

63

boundary points, as located by the program, are accurate only up to the point of maximum plume width. It must be remembered that the field method neglects the existence of the intercepting shock in the jet plume prior to the Mach disk. It is assumed that the expansion waves from the upper boundary pass through the intercepting shock undeflected. Although this will result in some error, it has been shown by Vick, et.al. [Ref. 12] that for:

$$\frac{P_j}{P_\infty} \leq 20,$$

very close agreement exists between the experimentally determined jet boundaries and those boundaries predicted by the MOC after ignoring the effect of the intercepting shock. Therefore, it is felt that the program will accurately locate the jet boundary up to the point of maximum plume width for jets which have a pressure ratio:

$$\frac{P_j}{P_\infty} ,$$

no greater than 20.

```
C
C
C             COMPUTER PROGRAM FOR LOCATING THE BOUNDARY
C                  OF AN UNDEREXPANDED FREE JET
C
C
C       N         IS THE NUMBER OF SUBDIVISIONS OF THE INITIAL
C                 EXPANSION FAN AT THE LIP OF THE NOZZLE.
C
C       NC        IS THE TOTAL NUMBER OF CELLS INTO WHICH THE
C                 FLOW IS SUBDIVIDED.
C
C       NOC       IS THE CELL NUMBER UP TO WHICH NO COMPRESSION
C                 WAVES HAVE BEEN CROSSED.
C
C       DELTA     IS THE TURNING ANGLE PER SUBDIVISIONS OF THE
C                 INITIAL EXPANSION FAN.  DELTA IS GIVEN IN
C                 DEGREES
C
C       THETA     IS THE FLOW INCLINATION IN A GIVEN CELL.
C                 THETA IS GIVEN IN DEGREES MEASURED COUNTER-
C                 CLOCKWISE FROM THE HORIZONTAL.
C
C       V         IS THE PRANDTL-MEYER ANGLE IN A GIVEN CELL,
C                 GIVEN IN DEGREES.
C
C       MU        IS THE MACH ANGLE GIVEN IN DEGREES
C
C       RR        IS THE DIRECTION OF THE RIGHT RUNNING
C                 CHARACTERISTIC GIVEN IN DEGREES.
C
C       LR        IS THE DIRECTION OF THE LEFT RUNNING
C                 CHARACTERISTIC GIVEN IN DEGREES.
C
C       CLPT      IS A POINT ON THE CENTER/LINE OF THE JET
C                 PLUME
C
C       BPT       IS A POINT ON THE BOUNDARY OF THE JET PLUME
C                 WHEN THE LETTER R APPEARS BEFORE OF AFTER A
C                 VARIABLE WHICH IS NORMALLY EXPRESSED AS AN
C                 ANGLE IN DEGREES, THIS NEW VARIABLE NAME IS
C                 NOW THE SAME ANGLE HOWEVER IT IS NOW IN TERMS
C                 OF RADIANS.
C                     FOR EXAMPLE:
C                       THETA   IS EXPRESSED IN DEGREES
C                       RTHETA  IS EXPRESSED IN RADIANS
C
C       REQUIRED DATA FOR THE PROGRAM.    ONE DATA CARD
C
C       PR        THIS IS THE RATIO OF THE JET TOTAL PRESSURE
C                 TO THE AMBIENT PRESSURE. THIS VALUE MUST BE
C                 EXPRESSED IN F FORMAT AND APPEAR IN THE
C                 FIRST TEN COLUMNS OF THE DATA CARD.
C
C       N         THIS IS AN INTEGER VALUE WHICH APPEARS RIGHT
C                 ADJUSTED IN COLUMNS 11-15 OF THE DATA CARD.
C
C
C                 THIS PROGRAM WILL HANDLE VALUE OF N WHICH
C                 ARE LESS THAN OR EQUAL TO 30.  IF IT IS
C                 DESIRED TO HAVE N LARGER THAN 30, THEN THE
C                 PROGRAM WILL HAVE TO BE REDIMINSIONED.
C
C
      INTEGER*4UE,CLPT,BPT
      REAL*4MACH,MU,LR,M2
      DIMENSION LE(1000),UE(1000),LC(1000),NX(100),NY(100),
     *NUM(100),THETA(1000),V(1000),C(200),D(200),BC(200),
     *FM(200),FMP(200),Z(200),DEL(200),MACH(1000),MU(1000),
     *RR(1000),LR(1000),X(1000),Y(1000),XB(100),YB(100)
```

65

```
      READ (5,1) PR,N
    1 FORMAT(F10.7,I5)
C
C
C     CALCULATE THE VALUE OF THE BOUNDARY MACH NUMBER.
C     EQN A-12    THE VARIABLE M2 IS THE SQUARE OF THE
C     BOUNDARY MACH NUMBER.
C
      TPR = 1./PR
      M2=5.*((TPR**(-.2857))-1)
C
C
C     CALCULATE THE INITIAL TURNING ANGLE (FTHETA).
C     EQN A-6 AND A-11
C
      VALUE=M2-1
      C1=SQRT(.166667*VALUE)
      C2=SQRT(VALUE)
      RTHETA=2.449*ATAN(C1)-ATAN(C2)
      FTHETA=RTHETA*57.29577
C
C
C
C     CALCULATE DELTA, THE FLOW DEFLECTION PER WAVE.
C
      DELTA=FTHETA/N
C
C     CALCULATE THE VALUES FOR NC AND NOC
C
C
      K=N-1
      SUM=0.0
      DO 5 I=1,K
      SUM=SUM+I
    5 CONTINUE
C
C
C     CALCULATE THE VALUES FOR NC AND NOC
C
      NOC=N**2 + N -SUM
      NC= N**2 + 2*N -1
C
C
C     SET THE VALUE OF LC FOR CELLS NUMBERING 1 TO NOC
C
      DO 10 I=1,NOC
      LC(I) = 0.0
   10 CONTINUE
C
C
C     SET THE VALUE OF LE FOR CELLS NUMBERING 1 TO NOC
C
      DO 20 I=1,N
      NX(1)=I
      NCELL=NX(1)
      LE(NCELL)=I
      J=I+1
      DO 15 L=2,J
      L1=L-1
      SUM=N-L+2
      NX(L)=NX(L1) + SUM
      NCELL=NX(L)
      LE(NCELL)=I
   15 CONTINUE
   20 CONTINUE
C
```

```
C
C         SET THE VALUE OF UE FOR CELLS NUMBERING 1 TO NOC
C
C
          NX(1) = 1
          NX(2) = 1 + N
          K = N+1
          DO 30 I=3,K
          L = I-2
          SUM = 0.0
          DO 25 J=1,L
          SUM = N-I+J+2+SUM
   25     CONTINUE
          NX(I) = 1+N+SUM
   30     CONTINUE
          NUM(1) = N
          NUM(2) = N
          DO 35 I=3,K
          NUM(I) = N-I+2
   35     CONTINUE
          DO 45 I=1,K
          NCELL = NX(I)
          UE(NCELL) = I-1
          J = NUM(I) -1
          IF(J.EQ.0) GO TO 45
          DO 40 L=1,J
          NCELL = NX(I) + L
          UE(NCELL) = I-1
   40     CONTINUE
   45     CONTINUE
C
C
C         SET THE VALUE OF LE FOR CELLS NUMBERING FROM NOC TO
C         NC
C
          DO 50 I=NOC,NC
          LE(I)=N
   50     CONTINUE
C
C
C         SET THE VALUE OF UE FOR CELLS NUMBERING FROM NOC TO
C         NC
C
          K=NOC+1
          NX(1)=K
          UE(K)=1
          DO 55 I=2,N
          JJ=I-1
          NX(I)=NX(JJ) + 1
          NAD=NX(I)
          UE(NAD)=I
   55     CONTINUE
          DO 70 I=2,N
          NUT=NX(I)
          K=I
          DO 65 J=2,K
          SUM=0.0
          MT=J
          DO 60 JK=2,MT
          SUM=SUM+N+1-JK
   60     CONTINUE
          NY(J)=NUT+SUM
          MAD=NY(J)
          UE(MAD)=I
   65     CONTINUE
   70     CONTINUE
C
C
C         SET THE VALUE OF LC FOR CELLS NUMBERING FROM NOC TO
C         NC
```

```
C
C
      NY(1)=NOC+1
      NUM(1)=N
      L=N-1
      DO 75 I=2,L
      J=I-1
      SUM=N-I+2
      NY(I)=NY(J)+SUM
      NUM(I)=N+1-I
   75 CONTINUE
      DO 85 I=1,L
      NCELL =NY(I)
      LC(NCELL)=I
      NL=NUM(I)-1
      DO 80 J=1,NL
      NCELL=NY(I)+J
      LC(NCELL)=I
   80 CONTINUE
   85 CONTINUE
C
C
C        CALCULATE THE VALUE OF THE PRANDTL-MEYER ANGLE FOR
C        EACH CELL ALONG WITH THE VALUE FOR THE LOCAL FLOW
C        DIRECTION THETA.    EQUATIONS A-14 AND A-15
C
C
      DO 90 I=1,NC
      THETA(I)=DELTA*(UE(I)-LE(I)+LC(I))
      V(I)=DELTA*(UE(I)+LE(I)-LC(I))
   90 CONTINUE
C
C
C        THE NEXT SECTION USES THE NEWTON-RAPHSON ITERATION
C        METHOD TO DETERMINE THE MACH NUMBER IN EACH CELL
C        GIVEN THE PRANDTL-MEYER ANGLE FOR THE CELL.  ONCE
C        THE MACH NUMBER IS KNOWN, THE MACH ANGLE (MU) AND THE
C        DIRECTIONS OF THE RIGHT RUNNING AND LEFT RUNNING
C        CHARACTERISTICS ARE CALCULATED FOR EACH CELL.
C
C
      A=2.4495
      B=0.40825
      E=0.001
      KEN=100
      DEL(1)=25.0
      DO 120 J=1,NC
      VR=0.0174532925*V(J)
      DO 105 K=1,10
      Z(1)=1.0+K/10.
      DO 100 I=1,KEN
      C(I)=SQRT(Z(I)**2-1.)
      D(I)=Z(I)*(1.+.2*Z(I)**2)
      BC(I)=B*C(I)
      FM(I)=A*ATAN(BC(I))-ATAN(C(I))-VR
      FMP(I)=C(I)/D(I)
      Z(I+1)=Z(I)-FM(I)/FMP(I)
      C(I+1)=SQRT(Z(I+1)**2-1.)
      BC(I+1)=B*C(I+1)
      FM(I+1)=A*ATAN(BC(I+1))-ATAN(C(I+1))-VR
      DEL(I+1)=ABS(Z(I+1)-Z(I))
      IF((DEL(I+1).LE.E).AND.(ABS(FM(I+1)).LE.E)) GO TO 110
      IF(DEL(I+1).GT.DEL(I)) GO TO 105
      IF(I.LE.KEN) GO TO 100
      GO TO 105
  100 CONTINUE
  105 CONTINUE
  110 MACH(J)=Z(I+1)
      RMU=ARSIN(1./MACH(J))
      MU(J)=RMU*57.29577
C
C
```

```
C       CALCULATE THE DIRECTIONS OF THE CHARACTERISTICS.
C       EQN. A-8 AND A-9
C
C
        RR(J)=THETA(J) - MU(J)
        LR(J)=THETA(J) + MU(J)
   120 CONTINUE
C
C
C       THE NEXT SECTION OF THIS PROGRAM CALCULATES THE
C       LOCATIONS OF ALL THE INTERSECTIONS OF THE EXPANSION
C       RAYS WITH THEIR OWN REFLECTIONS AND WITH THE CENTER
C       LINE
C
C
        CONV=57.2957795
        X(1)=0.0
        Y(1)=-1.0
        ANGR=(90+LR(1))/(2.*CONV)
        X(2)=1./TAN(ANGR)
        Y(2)=0.0
        CLPT=2
        P=1
        N1=N
        N2=2
        K=N-1
        LAST=CLPT+K
        JJ=CLPT+1
        DO 130 I=JJ,LAST
        N3=I-N2
        N4=I-N2+1
        N5=I-N2+N1
        AR=(LR(N3)+LR(N4))/(2.*CONV)
        BR=(RR(N3)+RR(N5))/(2.*CONV)
C
C
C       EQUATIONS A-18 AND A-19
C
        X(I)=(Y(I-1)-Y(P)+X(P)*TAN(AR)-X(I-1)*TAN(BR))/
       *(TAN(AR)-TAN(BR))
        Y(I)=(X(I)-X(P))*TAN(AR)+Y(P)
   130 CONTINUE
        P1= I+1
        P=P1-CLPT-1
        CLPT=P1
        N1=N1-1
        N2=N2-1
        K=K-1
        N6=CLPT-N2
        N7=N6+1
        AR=(LR(N6)+LR(N7))/(2.*CONV)
        NP=CLPT-N1
C
C
C       LOCATE CENTER-LINE POINT
C
        DELX=Y(NP)/TAN(AR)
        X(CLPT)=X(NP)+ABS(DELX)
        Y(CLPT)=0.0
        L=N-2
        DO 135 J=1,L
        LAST=CLPT+K
        JJ=CLPT+1
        DO 136 I=JJ,LAST
        N3=I-N2
        N4=N3+1
        N5=N3+N1
        AR=(LR(N3)+LR(N4))/(2.*CONV)
        BR=(RR(N3)+RR(N5))/(2.*CONV)
C
C
C       EQUATIONS A-18 AND A-19
C
        X(I)=(Y(I-1)-Y(I-P)+X(I-P)*TAN(AR)-X(I-1)*TAN(BR))/
       *(TAN(AR)-TAN(BR))
```

69
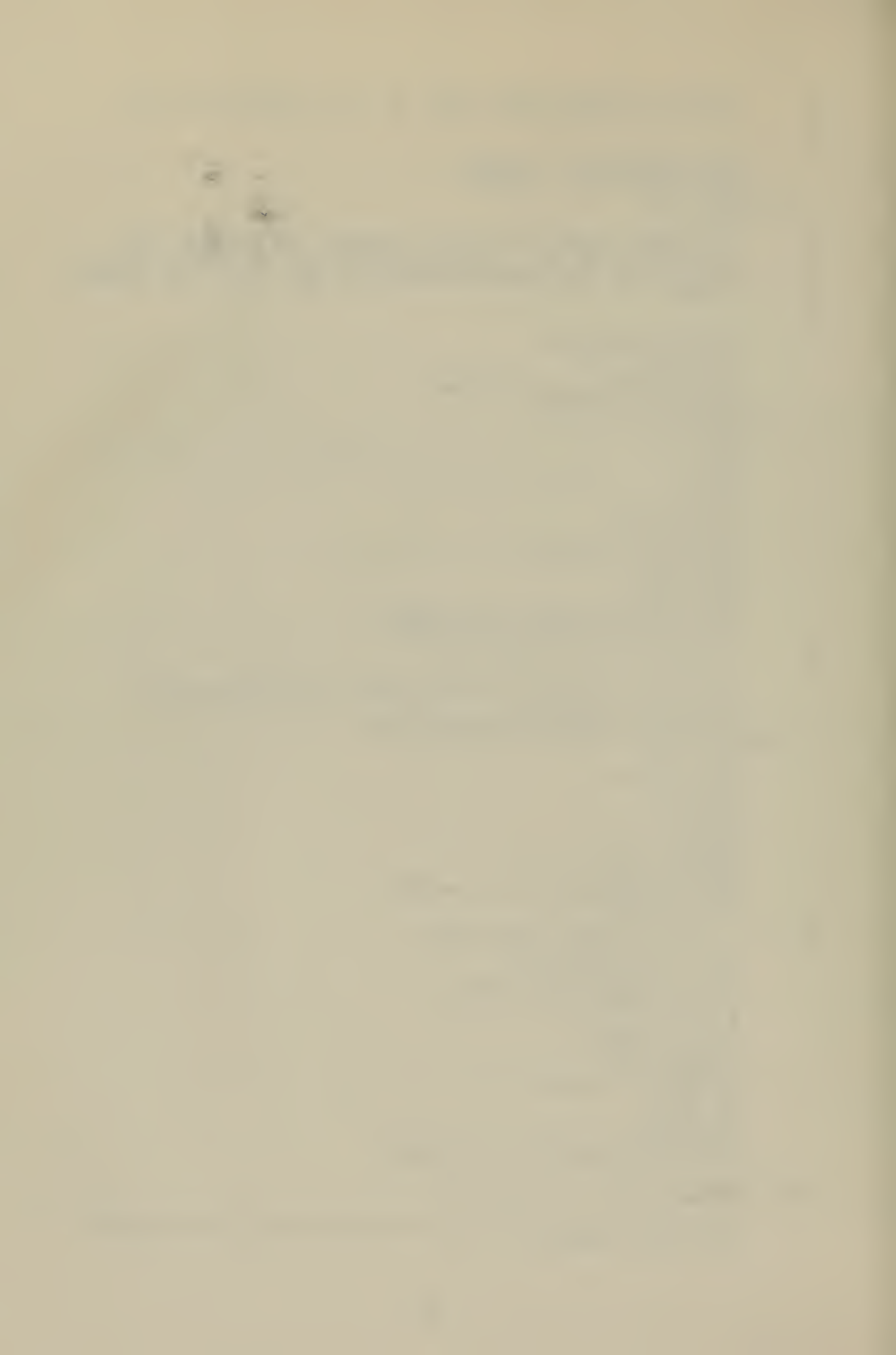
```
          Y(I)=(X(I)-X(I-P))*TAN(AR)+Y(I-P)
  136 CONTINUE
          P1=I+1
          P=P1-CLPT-1
          CLPT=P1
          N1=N1-1
          N2=N2-1
          K=K-1
          N6=CLPT-N2
          N7=N6+1
          AR=(LR(N6)+LR(N7))/(2.*CONV)
          NP=CLPT-N1
C
C       LOCATE CENTER-LINE POINT
C
          DELX=Y(NP)/TAN(AR)
          X(CLPT)=X(NP)+ABS(DELX)
          Y(CLPT)=0.0
  135 CONTINUE
          WRITE(6,500) FTHETA,N
  500 FORMAT('1','FTHETA =',F7.3,8X,'N =',I4,/////)
          WRITE(6,1000)
 1000 FORMAT(' ',        'CELL',6X,'LE ',6X,'UE ',6X,'LC ',6X
     *,'THETA',10X,'V',10X,'MACH',8X,'MU',10X,'RR',10X,
     *'LR',/////)
          DO 95 I=1,NC
          NCELL = I
          WRITE(6,2000) NCELL,LE(I),UE(I),LC(I),THETA(I),V(I),
     *MACH(I),MU(I),RR(I),LR(I)
 2000 FORMAT(' ',        I3,6X,I3,5X,I3,5X,I3,5X,F7.2,5X,F7.2
     *,5X,F7.2,5X,F7.2,5X,F7.2,5X,F7.2)
   95 CONTINUE
C
C
C       RENUMBER THE POINTS ON THE LAST EXPANSION RAY.
C       NUMBER 1 THROUGH N+1
C
C
          L=N+1
          J=1
          N1=N+1
          X(2)=X(N1)
          Y(2)=Y(N1)
          DO 145 I=3,L
          N1=N1+N-J
          X(I)=X(N1)
          Y(I)=Y(N1)
          J=J+1
  145 CONTINUE
C
C
C       CALCULATE THE LOCATION OF POINTS ALONG THE
C       COMPRESSION RAYS
C
          BPT=N+2
          N1=N
          N2=N1+N
C
C       LOCATE FIRST BOUNDARY POINT
C
          BR=(RR(N1)+RR(N2))/(2.*CONV)
          AR=THETA(N1)/CONV
          I=BPT
          X(I)=(Y(1)-Y(I-N)-X(1)*TAN(AR)+X(I-N)*TAN(BR))/
     *(TAN(BR)-TAN(AR))
          Y(I)=(X(I)-X(I-N))*TAN(BR)+Y(I-N)
          J=1
          N3=NOC+1
          II=I+1
          III=2*N+1
          DO 150 I=II,III
```

70

```
      N1=N2
      N2=N2+N-J
      AR=(LR(N1)+LR(N3))/(2.*CONV)
      BR=(RR(N1)+RR(N2))/(2.*CONV)
C
C        EQUATIONS A-18 AND A-19
C
      X(I)=(Y(I-1)-Y(I-N)-X(I-1)*TAN(AR)+X(I-N)*TAN(BR))/
     *(TAN(BR)-TAN(AR))
      Y(I)=(X(I)-X(I-N))*TAN(BR)+Y(I-N)
      J=J+1
      N3=N3+1
  150 CONTINUE
      N1=N1+2
      N2=N2+2
      P1=N
      P=N-1
      BPT=I+1
C
C        LOCATE BOUNDARY POINT
C
      BR=(RR(N1)+RR(N2))/(2.*CONV)
      AR=THETA(N1)/CONV
      I=BPT
      X(I)=(Y(I-P1)-Y(I-P)-X(I-P1)*TAN(AR)+X(I-P)*TAN(BR))/
     *(TAN(BR)-TAN(AR))
      Y(I)=(X(I)-X(I-P))*TAN(BR)+Y(I-P)
      K=N-2
      DO 175 J=1,K
      II=I+1
      III=II+P-2
      DO 170 I=II,III
      N1=N2
      N2=N2+1
      N3=N3+1
      AR=(LR(N1)+LR(N3))/(2.*CONV)
      BR=(RR(N1)+RR(N2))/(2.*CONV)
C
C        EQUATIONS A-18 AND A-19
C
      X(I)=(Y(I-1)-Y(I-P)-X(I-1)*TAN(AR)+X(I-P)*TAN(BR))/
     *(TAN(BR)-TAN(AR))
      Y(I)=(X(I)-X(I-P))*TAN(BR)+Y(I-P)
  170 CONTINUE
      BPT=I+1
      N1=N1+2
      N2=N2+2
      N3=N3+1
      P=P-1
      P1=P1-1
C
C        LOCATE BOUNDARY POINT
C
      BR=(RR(N1)+RR(N2))/(2.*CONV)
      AR=THETA(N1)/CONV
      I=BPT
      X(I)=(Y(I-P1)-Y(I-P)-X(I-P1)*TAN(AR)+X(I-P)*TAN(BR))/
     *(TAN(BR)-TAN(AR))
      Y(I)=(X(I)-X(I-P))*TAN(BR)+Y(I-P)
  175 CONTINUE
C
C
C        THIS SECTION DETERMINES WHICH OF THE CALCULATED
C        POINTS ARE BOUNDARY POINTS AND PRINTS THEM OUT IN A
C        SEPARATE LISTING.
C
      SUM=1.0
      DO 180 J=1,N
      SUM=N+2-J+SUM
      BPT=SUM
      X(J+1)=X(BPT)
```

71

```fortran
      Y(J+1)=Y(BPT)
  180 CONTINUE
      WRITE(6,4300) TPR,PR,N
 4300 FORMAT('1',17X,'BOUNDARY POINTS NONDIMENSICNALIZED BY
     *SLOT WIDTH',//,18X,'PRESSURE RATIO =',F9.7,4X,'(',
     *F5.2,')',//,18X,'N =',I4,///,20X,'X/SW',10X,'Y/SW',
     *//////)
      II=N+1
      DO 185 I=1,II
      X(I)=X(I)/2.
      Y(I)=Y(I)/2.
      WRITE(6,4500) X(I),Y(I)
 4500 FORMAT(' ',17X,F7.3,4X,F7.3)
  185 CONTINUE
      STOP
      END
```

72

REFERENCES

1. Manoury, F., Kadosch, M., and Bertin, J., "Contròle par le jet transversal de la section d'éjection des tuyeres à réaction," C.R. Acad. Sci. Paris, vol. 8, pp. 623-624.

2. Martin, A.I., "The Aerodynamic Variable Nozzle," J. of the Aero/ Space Sci., vol. 24, no. 5, pp. 357-362. May 1957

3. McArdle, J.G., Internal Characteristics and Performance of an Aerodynamically Controlled Variable-Discharge Coefficient Nozzle, NACA, TN 4317, July 1958.

4. Zumwalt, G.W., and Jackomis, W.N., "Aerodynamic Throat Nozzle for Thrust Magnitude Control of Solid Fuel Rockets," ARS J., vol. 32, no. 12, pp. 1934-1936, December 1962.

5. Gardiner, R.E., Secondary Injection for Solid Rocket Thrust Magnitude Control, MS Thesis, College of Aeronautical and Astronautical Engineering, University of Illinois, 1964.

6. Nunn, R.H., Aerodynamic Throttling and Jet Penetration, Ph.D. Thesis, Mechanical Engineering Department, University of California, Davis, 1967.

7. Warinner, D.K., Jet Attachment in Aerodynamic Throttling, MS Thesis, Mechanical Engineering Department, University of California, Davis, 1965.

8. Schetz, J.A., and Billig, F.S., "Penetration of Gaseous Jets Injected into a Supersonic Stream," J. of Spacecraft and Rockets, vol. 3, no. 11, pp. 1658-1665, Nov. 1966.

9. Orth, R.C., and Funk, J.A., "An Experimental and Comparative Study of Jet Penetration in Supersonic Flow," J. of Spacecraft and Rockets,, vol. 4, no. 9, pp. 1236-1242, September 1967.

10. Barnes, J.W., David, J.G., and Tang, H.H., Control Effectiveness of Transverse Jets Interacting with a High-Speed Free Stream, Air Force Flight Dynamics Laboratory, AFFDL-TR-67-90, vol. I, September 1967.

11. Spaid, F.W., and Zukoski, E.E., "A study of the Interaction of Gaseous Jets from Transverse Slots with Supersonic External Flows," AIAA J., vol. 6, no. 2, pp. 205-212, February 1968

12. Vick, A.R., Andrews, E.H., Jr., Dennard, J.S., and Craidon, C.B., Comparisons of Experimental Free-Jet Boundaries with Theoretical Results Obtained with the Method of Characteristics, NASA TN D-2327, June 1964.

13. Vaughan, J.C., III, "A Two-Dimensional Study of the Jet Interaction and downstream Burning Resulting from a Gaseous Sidejet Expanding Into a Supersonic Airstream," <u>Jet Propulsion Center</u>, Purdue University, Rep No. TM-70-5, June 1970.

14. Maurer, F., "Interference Effects Produced by Gaseous Side-Jets Issuing into a Supersonic Stream," <u>Applied Physics Lab.</u> Library Bulletin Transl., Ser. TC 230-T 460, November 1965.

15. Nunn, R.H., and Brandt, H., "Aerodynamic Throttling of Two-Dimensional Nozzle Flows," To be published in Aeronautical Quarterly.

16. Adamson, T.C., Jr., and Nicholls, J.A., "On the Structure of Jets from Highly Underexpanded Nozzles into Still Air," <u>J. of the Aero/Space Sci.</u>, vol. 26, no. 1, pp. 16-24, January 1959.

17. Cassel, L.A., Davis, J.G., and Tang, H.H., <u>Lateral Jet Control Effectiveness Prediction for Axisymmetric Missile Configurations</u>, U.S. Army Missile Command, Rep. No. RD-TR-68-5, June 1968

18. ASME, Flow Measurement, Chapter 4, part 5 of Instrumentations and Apparatus Supplement to the ASME Power Test Codes, PTC 19.5; 4-1959, New York, Feb. 1959.

19. Rotty, R.M., <u>Introduction to Gas Dynamics</u>, New York, John Wiley and Sons, Inc., 1962.

INITIAL DISTRIBUTION LIST

No. Copies

1. Defense Documentation Center   2
    Cameron Station
    Alexandria, Virginia 22314

2. Library, Code 0212   2
    Naval Postgraduate School
    Monterey, California 93940

3. Assoc. Professor R. H. Nunn, Code 59 Nn   1
    Mechanical Engineering Department
    Naval Postgraduate School
    Monterey, California 93940

4. LT. Kenneth Edwin Frick, USN   1
    1576 Maple Road
    Cleveland Heights, Ohio 44121

5. Department of Mechanical Engineering   1
    Naval Postgraduate School
    Monterey, California 93940
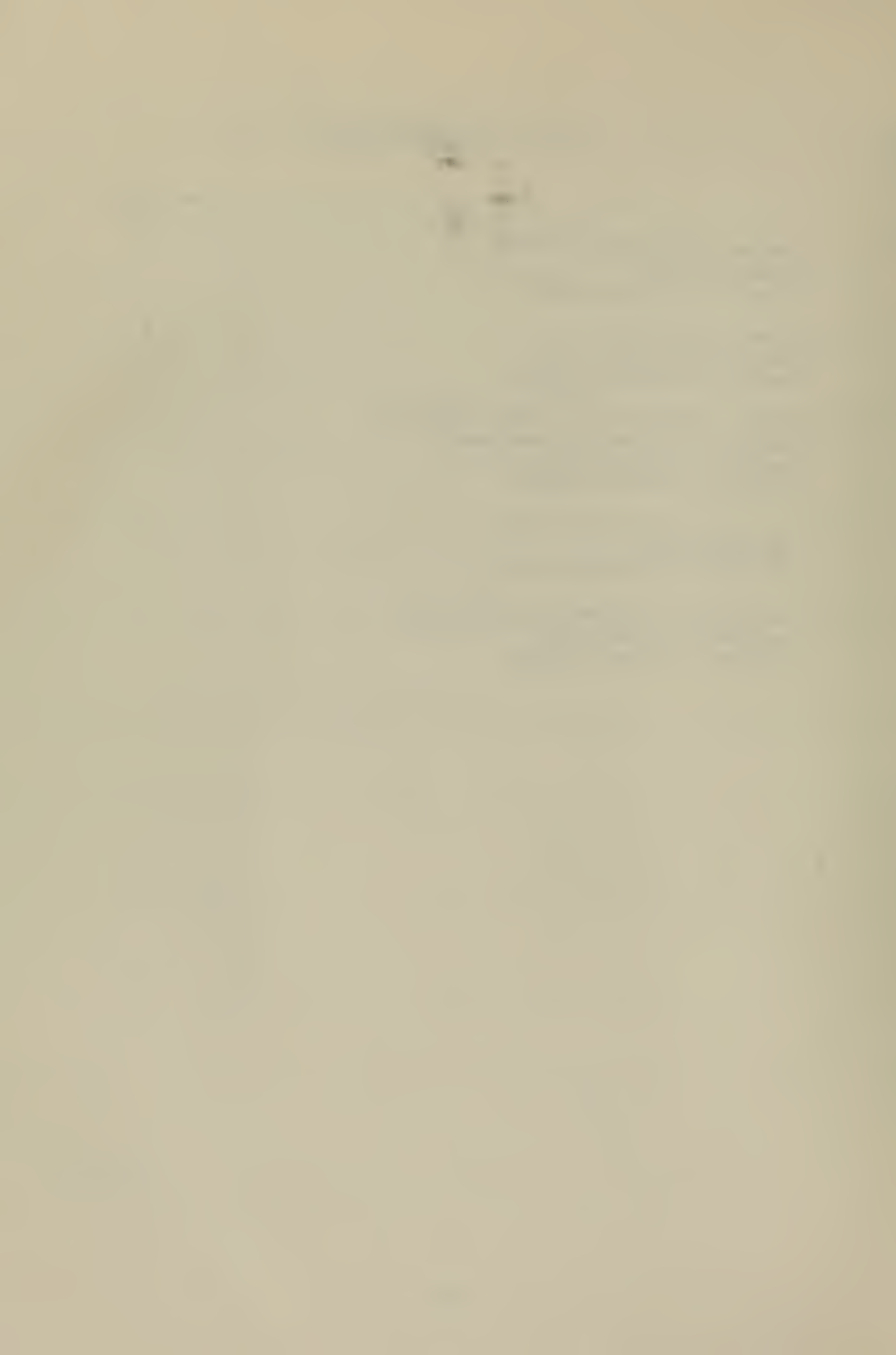
DOCUMENT CONTROL DATA - R & D

(Security classification of title, body of abstract and indexing annotation must be entered when the overall report is classified)

1. ORIGINATING ACTIVITY *(Corporate author)*	2a. REPORT SECURITY CLASSIFICATION
Naval Postgraduate School Monterey, California 93940	Unclassified
	2b. GROUP

3. REPORT TITLE

Jet Penetration and Interaction at a Sonic Throat

4. DESCRIPTIVE NOTES *(Type of report and inclusive dates)*
Master's Thesis; March 1972

5. AUTHOR(S) *(First name, middle initial, last name)*

Kenneth Edwin Frick

6. REPORT DATE	7a. TOTAL NO. OF PAGES	7b. NO. OF REFS
March 1972	77	19

8a. CONTRACT OR GRANT NO.	9a. ORIGINATOR'S REPORT NUMBER(S)
b. PROJECT NO.	
c.	9b. OTHER REPORT NO(S) *(Any other numbers that may be assigned this report)*
d.	

10. DISTRIBUTION STATEMENT

Approved for public release; distribution unlimited.

11. SUPPLEMENTARY NOTES	12. SPONSORING MILITARY ACTIVITY
	Naval Postgraduate School Monterey, California 93940

13. ABSTRACT

This thesis describes the results of an investigation of the throttling effects of a transverse jet when injected into a sonic throat. The process, commonly referred to as aerodynamic throttling, was studied both analytically and experimentally.

An analytical model is developed utilizing momentum considerations. This model successfully predicts the measured throttling results for 90° injection and mainstream flow reductions up to approximately 60 percent. The agreement between theory and experiment becomes less satisfactory as the upstream angle of injection is increased and at extremely high throttling conditions.

An experimental program is described in which a two-dimensional nitrogen jet is injected into the mainstream through slots of various widths and inclinations. Visual flow patterns are shown to qualitatively describe the nature of the interaction between the jet and the mainstream.

DD FORM 1473 (PAGE 1)
I NOV 65

S/N 0101-807-6811

A-31408

14. KEY WORDS	LINK A		LINK B		LINK C	
	ROLE	WT	ROLE	WT	ROLE	WT
Jet Interaction						
Aerodynamic Throttling						